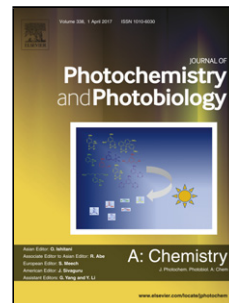


Accepted Manuscript

Title: Synthesis, Characterization, DNA Binding and Cleaving Properties of Photochemically Activated Phenanthrene Dihydrodioxin

Author: Anastasiia A. Tikhomirova Nikolai A. Tcyrulnikov
R. Marshall Wilson



PII: S1010-6030(18)31646-0
DOI: <https://doi.org/doi:10.1016/j.jphotochem.2019.04.014>
Reference: JPC 11803

To appear in: *Journal of Photochemistry and Photobiology A: Chemistry*

Received date: 14 November 2018
Revised date: 24 March 2019
Accepted date: 10 April 2019

Please cite this article as: A.A. Tikhomirova, N.A. Tcyrulnikov, R.M. Wilson, Synthesis, Characterization, DNA Binding and Cleaving Properties of Photochemically Activated Phenanthrene Dihydrodioxin, *Journal of Photochemistry and Photobiology A: Chemistry* (2019), <https://doi.org/10.1016/j.jphotochem.2019.04.014>

This is a PDF file of an unedited manuscript that has been accepted for publication. As a service to our customers we are providing this early version of the manuscript. The manuscript will undergo copyediting, typesetting, and review of the resulting proof before it is published in its final form. Please note that during the production process errors may be discovered which could affect the content, and all legal disclaimers that apply to the journal pertain.

Synthesis, Characterization, DNA Binding and Cleaving Properties of Photochemically Activated Phenanthrene Dihydrodioxin

Anastasiia A. Tikhomirova, Nikolai A. Tcyrulnikov, R. Marshall Wilson

Center for Pure and Applied Photosciences, Bowling Green State University, Bowling Green, OH 43403, USA

1. Introduction

DNA molecule remains the most desirable target in anticancer studies [1]. Thus, the design and characterization of DNA binding and cleaving agents have been an active area of research for decades [2]. Small molecules can bind to DNA through covalent and non-covalent interactions [3]. The latter includes three different binding modes: electrostatic interactions with the phosphate backbone, intercalation between DNA base pairs, and groove binding [4]. Among these interactions, intercalating binding proved to be one of the most efficient modes for the development of DNA targeting compounds [5]. Intercalators are small organic molecules with planar aromatic moieties that insert between DNA base pairs resulting in the modification of the native DNA structure [6]. The accommodation of an intercalator induces a crucial perturbation in the DNA molecule: it unwinds the helical twist and causes DNA lengthening [7]. This deformation might result in the vital errors in such important biological functions as DNA replication and transcription [8]. Thus, intercalators represent a promising class of compounds that are used as lead structures for anticancer drugs design [9].

In addition to a distortion of a DNA molecule caused by the intercalation, either thermal or photoinduced damage can be caused by DNA cleaving agents. Photoswitchable DNA cleavers were most accurately described by Armitage as ‘compounds whose excited states can initiate a series of chemical reactions which ultimately lead to nucleic acid cleavage’ [10]. DNA photocleavers typically absorb at a wavelength longer than 300 nm [11] – the region where

nucleic acids and the majority of proteins are transparent, which helps to selectively excite a photocleavage agent. Photoswitchable DNA damaging agents have a number of advantages over the thermally activated compounds [12]. Among these advantages is the prior binding of a photocleaver to DNA molecule before the irradiation and ‘light-clicking’ reaction management: light allows to control the reaction in both spatial and temporal ways [13]. These unique properties have triggered the search for efficient DNA photocleaving agents. Although photoswitchable ligand complexes of transition metals have been thoroughly investigated and their design still remains an extensive research area [14], smaller number of studies cover ‘light-clicking’ small organic molecules capable of intercalating in DNA structure. Examples of photoactivated organic compounds include, for instance, enediynes [15], naphthalimide [16] and pyrene derivatives [17].

Herein, in continuation of our interest in designing new DNA photocleavage agents [18], we report the synthesis, characterization and DNA binding and cleaving properties of a novel compound: *trans-N,N*-dimethyl-10,11-di(pyridin-4-ium)-10,11-dihydro-9,12-dioxobenzo[e]phenanthrene tetrafluoroborate (**1**). As early as in 1947, it was shown by Schönberg that 9,10-phenanthrenequinone and other *ortho*-quinone derivatives form a dihydrodioxin photoproduct when mixed with substituted alkenes under visible light irradiation [19]. Exposure of dihydrodioxin solutions to UV light can result in the reverse reaction of the photochemical release of the *ortho*-quinone and corresponding alkene [20]. This reaction, therefore, was successfully implemented to photochemically mask highly reactive *ortho*-quinone species [18, 21]. It is known that 9,10-phenanthrenequinone, a component of diesel exhaust particles – carcinogenic air pollutant, can induce the oxidative DNA damage by enhancing the production of reactive oxygen species [22]. The mechanism of the *ortho*-quinone release was

investigated in previous studies [18, 23] in which the formation of an *ortho*-quinone radical anion, dihydrodioxin radical cation and Reactive Oxygen Species (ROS) was demonstrated. These species are well known to cause oxidative DNA damage, which may additionally contribute to DNA damaging properties of **1** [18, 20, 21, 22, 24]. The interaction of **1** with DNA was described by a number of spectroscopic analytical tools, such as UV-Vis absorption (DNA titration and DNA optical melting experiments), circular dichroism (CD) and fluorescence. Intercalative binding mode of **1** was unambiguously demonstrated by viscometric analysis. Photolysis of the compound in question with both visible and UV light was performed to better understand the photochemistry of **1** that is involved in DNA cleavage. Φ X 174 photocleavage assay was used to evaluate DNA damage triggered by **1**.

Main advantages of pyridinium containing dihydrodioxins are: a) ease of synthetic preparation from commercially available compounds; b) dihydrodioxins present a masked form of reactive *ortho*-quinones, release of which can be controlled by irradiation by different wavelengths of light; c) phenanthrene dihydrodioxin has a higher solubility in biological media comparing to the previously studied more hydrophobic pyrene dihydrodioxin derivative [18]; d) combination of flat aromatic moiety with positively charged pyridinium rings allows for both intercalative and electrostatic interactions of **1** with DNA.

2. Experimental

2.1 Materials and methods

All reagents and solvents were used as received from chemical suppliers with no additional purification unless otherwise noted. Moisture sensitive reactions were performed under an atmosphere of argon in glassware that was flame-dried under high vacuum. Moisture

sensitive reagents were handled in a glovebox in an atmosphere of nitrogen. UltraPure Calf Thymus DNA (CT-DNA, 10 mg/mL) solution was purchased from Fisher. Dilution of the CT-DNA stock solution was performed using BioPerformance Certified water (Sigma-Aldrich). Concentrations of all CT-DNA solutions were calculated in the concentration of base pairs (bp), using the extinction coefficient of $13200 \text{ bp cm}^{-1} \text{ M}^{-1}$ at 260 nm [25]. The purity of CT-DNA was confirmed by high A_{260}/A_{280} ratio (1.9), which is a strong indication of a negligible presence of proteins in CT-DNA solution [26]. All DNA experiments were performed in 10 mM Phosphate Buffer (PB) solution of pH 7.4 (2 mM NaH_2PO_4 , Sigma-Aldrich, anhydrous, BioPerformance Certified, >99 %; 8 mM Na_2HPO_4 , Sigma-Aldrich, anhydrous, BioXtra, >99%) with 100 mM NaCl (Sigma-Aldrich, BioXtra, >99%) added. BioPerformance Certified water was used for buffers preparation.

Double-stranded DNA oligonucleotides (Integrated DNA Technologies) used in the current work included the following sequences (one strand is shown): 5'– ATCGACCAAGC – 3' (11-mer, 54.5 % of GC content); 5' – GTTAGTATATGG – 3' (12-mer, 33.3 % of GC content); 5' – GCCGCGCGCGG – 3' (11-mer, *polyGC*); 5' – ATATATATATA – 3' (11-mer, *polyAT*). All samples were purified by Polyacrylamide Gel Electrophoresis (PAGE) procedure [27] by the supplier. DNA oligonucleotides were stored at $-20 \text{ }^\circ\text{C}$. To prepare DNA oligonucleotides stock solutions, the samples were thawed at room temperature, stirred and dissolved in BioPerformance Certified water. Concentrations of stock solutions were calculated using the exact molar amounts and extinction coefficients (see SI) of double-stranded DNA oligonucleotides provided by the supplier.

Proton and carbon NMR were recorded on a Bruker Avance III 500 Spectrometer equipped with cryoprobe using tetramethylsilane (TMS) or residual solvent peak as the internal

standard. IR spectra were recorded on Thermo Scientific Nicolet iS5 ATR IR Spectrometer. Mass spectrometry data were obtained on a cyclotron resonance Fourier Transform MS using electrospray ionization.

2.2 Synthesis of *trans*-10,11-di(pyridin-4-yl)-10,11-dihydro-9,12-dioxobenzo[*e*]phenanthrene

To 9,10-Phenanthrenequinone (Sigma-Aldrich, > 99%, 0.52 g, 2.49 mmol) solution in 160 mL of benzene was added a two-fold excess of 1,2-di(4-pyridyl)ethylene (Sigma-Aldrich, 97%, 0.91 g, 5.00 mmol). After all reaction components were completely dissolved, the bright yellow solution was transferred into a photochemical reaction vessel equipped with a gas dispersion tube with a porous fritted glass tip. The reaction mixture was purged with argon for 1.5 hours and then placed into a photoreactor. The reaction vessel was irradiated by 419 nm lamps (Southern New England Ultraviolet Company) inside the photoreactor with constant stirring and argon purging for 3 hours at 20 °C (the temperature maintained by Haake A82 Temperature Bath / Recirculator filled with ethanol). After 3 hours, the gas dispersion tube was removed, and the photochemical reaction vessel was tightly closed with a stopper for continuous overnight irradiation. After the overnight reaction, the solvent from the resulting pale yellow solution was evaporated under reduced pressure followed by the addition of 160 mL of methanol. The immediate formation of the off-white precipitate was observed. The reaction mixture was kept in the dark for 12 hours at 0 °C. The precipitate was filtered and thoroughly washed with methanol and diethyl ether to afford off-white crystals. Further recrystallization of the solid from acetone gave *trans*-10,11-di(pyridin-4-yl)-10,11-dihydro-9,12-dioxobenzo[*e*]phenanthrene as an off-white fine crystalline powder (0.26 g, 26 %). Mp = 207-210 °C (decomp.) ¹H NMR (500 MHz, CDCl₃) δ 8.67 (d, *J* = 9.44 Hz, 2 H), 8.60 (d, *J* = 6.01 Hz,

4 H), 8.22 (d, $J = 9.45$ Hz, 2 H), 7.65-7.62 (m, 4 H), 7.12 (d, $J = 6.03$ Hz, 4 H), 5.09 (s, 2 H). ^{13}C NMR (125 MHz, CDCl_3) δ 150.13, 144.3, 133.3, 127.0, 126.9, 125.7, 125.6, 122.7, 122.4, 120.8, 79.2. IR ($\nu = \text{cm}^{-1}$): 3031, 1600, 1450, 1325, 1248, 1112, 1038, 976, 825, 721, 655, 551. HRMS (ESI): m/z calcd. for $\text{C}_{26}\text{H}_{19}\text{N}_2\text{O}_2^+ [\text{M}^+]$, 391.14410, found 391.14410.

2.3. *Synthesis of trans-N,N-dimethyl-10,11-di(pyridin-4-ium)-10,11-dihydro-9,12-dioxobenzo[e]phenanthrene tetrafluoroborate (1)*

To a stirred solution of *trans*-10,11-di(pyridin-4-yl)-10,11-dihydro-9,12-dioxobenzo[e]phenanthrene (0.57 g, 0.15 mmol) in 160 mL of dichloromethane (freshly distilled from P_2O_5) was added an excess of trimethyloxonium tetrafluoroborate (Sigma-Aldrich, 95%, 0.14 g, 0.97 mmol). The reaction mixture was stirred at the boiling temperature of dichloromethane for 3 days under an argon atmosphere. After 3 days, the formation of fine pale yellow crystals was observed. After cooling to room temperature, most of the solvent was evaporated under reduced pressure leaving approximately 30 mL of the suspension in the flask. This light brown suspension was cooled down to 0 °C in an ice bath, vacuum-filtered and liberally washed with dichloromethane and a few small portions of diethyl ether. The precipitate obtained was additionally purified by recrystallization from the chloroform/methanol mixture (5:1) to afford **1** as a pale yellow crystalline powder (0.62 g, 69 %). Mp = 228-230 °C (decomp.) ^1H NMR (500 MHz, CD_3CN) δ 8.75 (dd, $J = 7.86, 1.3$ Hz, 2 H), 8.57 (d, $J = 6.61$ Hz, 4 H), 8.21 (dd, $J = 9.35, 1.7$ Hz, 2 H), 8.03 (d, $J = 6.53$ Hz, 4 H), 7.76-7.61 (m, 4 H), 6.20 (s, 2 H), 4.25 (s, 6 H). ^{13}C NMR (125 MHz, CD_3CN) δ 155.5, 146.8, 133.0, 128.7, 128.3, 127.5, 127.1, 126.0, 124.1, 121.5, 76.1, 49.2. IR ($\nu = \text{cm}^{-1}$): 3078, 1637, 1501, 1457, 1338, 1287, 1191, 1038, 975, 845, 763, 520. HRMS (ESI): m/z calcd. for $\text{C}_{28}\text{H}_{24}\text{N}_2\text{O}_2^{2+} [\text{M}^{2+}]$, 420.18268, found 420.18266; m/z calcd. for $\text{C}_{28}\text{H}_{24}\text{N}_2\text{O}_2\text{BF}_4^+ [\text{M}^{2+} \cdot \text{BF}_4^-]$, 507.18615, found 507.18604.

2.4 Photolysis of **1**

Acetonitrile solution of **1** in 1 cm quartz cuvette (Starna Cells) equipped with a screw cap was placed inside a photoreactor and irradiated by 350 nm UV lamps. The changes in the UV spectrum of **1** were monitored every 20 s during a 5 min. time period, every 30 s during a 15 min. time period, and every 60 s within a 5 min. time period and recorded on an Agilent Technologies UV-Vis spectrometer. Irradiation of **1** in acetonitrile by 419 nm photochemical lamps was performed according to the same procedure. The concentration of **1** in acetonitrile was calculated from the absorbance at 305 nm and the extinction coefficient determined by Beer's law ($\epsilon_{305} = 11150 \text{ cm}^{-1} \text{ M}^{-1}$).

2.5 Studies of interaction of **1** with DNA

2.5.1 Viscosity measurements

Measurements were performed using Ostwald type viscometer (Thomas PHILA, USA) at $(24.0 \pm 0.1) ^\circ\text{C}$. A 1 mM solution of CT-DNA base pairs was prepared in 10 mM PB solution with 100 mM NaCl and transferred into the viscometer and equilibrated to $24 ^\circ\text{C}$ during 5 minutes. The flow-time of CT-DNA solution was measured by digital stopwatch 4 times until the flow times fell within ± 0.5 s. The CT-DNA solution was then titrated by incremental additions of 6.74 mM stock solution of **1** in DMSO. The solution of **1** was prepared in DMSO due to the lower solubility of the studied compound in aqueous media. After each addition of **1** the resulting solution in the viscometer was mixed by repeated gentle air suction with a disposable syringe connected to the rubber tube, and then the solution was equilibrated to $24 ^\circ\text{C}$ for approximately 5 minutes. The average flow-time after each addition of **1** was calculated based on at least 3 flow-time measurements the results of which fell within ± 0.5 s. To evaluate the effect of the additions

of the organic solvent (DMSO) on the viscosity of the DNA solution, 2 additional series of the control titrations were performed: 1) the flow-times of the 10 mM PB solution with 100 mM NaCl itself and with incremental additions of pure DMSO were measured; 2) the flow-times of the 1 mM CT-DNA solution in 10 mM PB with 100 mM NaCl itself and with incremental additions of pure DMSO were determined.

The viscosity of CT-DNA solution before the addition of **1** was calculated according to the formula $\eta_o = (t - t_o)/t_o$ where t_o – flow-time of the buffer without CT-DNA and t – flow-time of the buffer with CT-DNA added. To calculate the viscosities of the CT-DNA solution upon incremental additions of **1**, the following equation was utilized $\eta = (t_1 - t_o)/t_o$ where t_1 – flow-time of the CT-DNA solution with DMSO solution of **1** added. The effect of the organic solvent on the viscosity of the CT-DNA solution was considered and the viscosities values were corrected by using the flow-times of the PB (t_o) and CT-DNA (t) solutions from the control titrations with pure DMSO. The results of viscometric titrations of the CT-DNA solution by **1** were presented as relative viscosity of CT-DNA, $(\eta/\eta_o)^{1/3}$, plotted vs the ratio of molecules of **1** to the base pairs of CT-DNA, r (**1**/CT-DNA) [28].

2.5.2 UV-Vis titration

DNA binding was studied by monitoring changes of the UV-Vis absorption spectrum of **1** upon addition of double-stranded DNA oligonucleotides: 11-mer, *polyGC*, *polyAT*. Absorption spectra were recorded in the 200-600 nm range on an Agilent Technologies UV-Vis spectrometer. PB solutions with a constant concentration of **1** (20-30 μ M) was used in each experiment, for exact concentrations see SI) in 1 cm quartz cuvette were titrated by incremental additions of the DNA solutions until no further absorption changes of **1** were observed. After each DNA addition, the cuvette was stirred for 60 s. The concentration of **1** in PB was calculated

from the absorbance at 305 nm and extinction coefficient determined experimentally ($\epsilon_{305} = 8979 \text{ cm}^{-1} \text{ M}^{-1}$).

Binding constants were determined by plotting the difference in apparent extinction coefficient of the DNA binder in question *vs* DNA oligonucleotides concentration [29]. The following equation of a half-reciprocal plot was used [30]

$$\frac{[\text{DNA}]}{\Delta\epsilon_{\text{app}}} = \frac{[\text{DNA}]}{\Delta\epsilon} + \frac{1}{\Delta\epsilon K} \quad (1)$$

where $\Delta\epsilon_{\text{app}} = |\epsilon_a - \epsilon_f|$, $\Delta\epsilon = |\epsilon_b - \epsilon_f|$, and ϵ_a , ϵ_f and ϵ_b are apparent, free (unbound) and bound extinction coefficient of the DNA binder, correspondingly; $[\text{DNA}]$ – molar concentration of DNA oligonucleotides in solution, K – equilibrium binding constant of DNA with **1**. The slope of the $[\text{DNA}]/\Delta\epsilon_{\text{app}}$ *vs.* $[\text{DNA}]$ plot equals to $1/\Delta\epsilon$, while Y-axis intercept is equivalent to $1/\Delta\epsilon K$. DNA binding constant is therefore defined as the ratio of the graph slope to the intercept.

2.5.3 UV-Vis optical melting experiments

Melting curves were recorded in the absence and presence of incremental additions of **1**. DNA absorbance at 260 nm was monitored on Cary-Bio UV–Vis spectrophotometer (Varian Inc.) equipped with a thermo controlling cell. Solutions of DNA oligonucleotides in 1 cm quartz cuvette were thermostated at 20 °C for 3 min. Stirred solutions were heated from 20 °C to 60 °C at 0.5 °C/min. rate. Melting temperatures of pure DNA oligonucleotides, T_m (DNA), and in the presence of the binder, T_m (DNA-binder), were determined from the first derivative curves (dA_{260}/dT *vs* T). Shifts in DNA melting temperatures, ΔT_m , induced by the addition of **1** were evaluated as the difference between the melting temperature of the DNA-binder mixture and the melting temperature of the DNA itself.

2.5.4 Circular Dichroism (CD) spectroscopy

A solution of CT-DNA (30 μM) in 1 cm quartz cuvette was placed in thermoelectrically controlled cell holder of an AVIV 62DS Circular Dichroism Spectrometer. Spectra of CT-DNA solution itself and solutions of CT-DNA with increasing amounts of **1** were recorded under a nitrogen atmosphere at 22.5 $^{\circ}\text{C}$. Addition of the DNA binder continued until no further change in the CD spectrum of CT-DNA was observed [31]. CD changes of the CT-DNA solutions were monitored in the 190-350 nm range.

2.5.5 Fluorescence measurements

A solution of **1** (33 μM) in PB was excited at the 308 nm isosbestic point. Emission spectra of **1** itself and its mixtures with 11 μM CT-DNA were recorded. After CT-DNA addition the sample was stirred for 180 s. Fluorescence intensities were monitored at 410 nm. Measurements were taken in 1 cm quartz cuvette at room temperature on Edinburgh FLS920-stm steady state spectrofluorimeter (Edinburgh Instruments). Emission was monitored in 360-520 nm range.

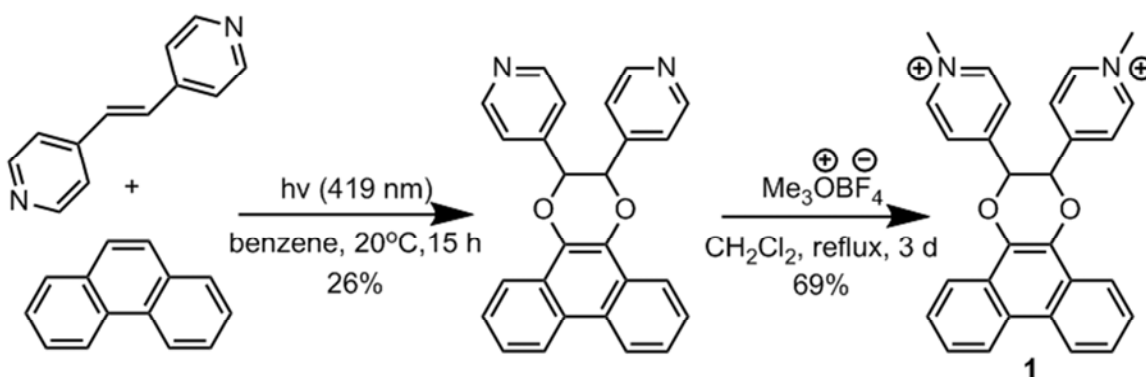
2.6 ΦX174 photocleavage assay

A solution of 0.5 μL ΦX174 RF I DNA (1 mg/mL, 5386 base pairs length, New England Biolabs (NEB) was transferred in a 0.6 mL Eppendorf tube (Fisher Scientific, 02-681-300). Then 1 μL of PB solution of **1** of the required concentration was added to the tube and stirred. Three different concentrations of **1** were used: 1 molecule of **1** per 50 base pairs of ΦX174 RF I DNA (1:50 bp), 1:10 bp and 1:2 bp. The samples were incubated in the dark for 10 minutes. After incubation, each sample was placed at the 20 cm distance from a He/Cd CW laser (56 series Melles Griot Co, 70 mW) and irradiated by 442 nm light. Irradiation was performed for up to 60

minutes in 15 minutes intervals. After irradiation, samples were diluted with 10 μ L of PB. DNA photocleavage was visualized by gel electrophoresis (1 % agarose gel prestained with 0.01% of GelRed Nucleic Acid Stain, (Biotium) /1X TAE buffer/Blue Juice Loading dye (Thermo Fisher)/1kb DNA ladder (NEB). Typically gel electrophoresis was run for approximately 3 hours at 60 V. Gels were visualized using a 302 nm transilluminator (TR-302, Ultraviolet) and photographed by a digital camera through an ethidium bromide filter. Densitometric analysis of the DNA bands was performed in Image Studio Lite software.

3. Results and discussion

3.1 Photolysis of **1**



Scheme 1. Synthesis and structure of **1**.

Phenanthrene dihydrodioxin **1** was synthesized based on the Schönberg-Mustafa reaction followed by the methylation reaction to produce the final pyridinium salt photoproduct (Scheme 1). To analyze the photochemical properties of **1** and to monitor the 9,10-phenanthrenequinone release, we performed steady-state photolysis using both UV (350 nm) and visible light (419 nm) irradiation. Extinction coefficients of **1** in acetonitrile at two different irradiation wavelengths were determined experimentally as $\epsilon_{350} = 1960 \text{ cm}^{-1} \text{ M}^{-1}$ and $\epsilon_{419} = 550 \text{ cm}^{-1} \text{ M}^{-1}$. The 9,10-

phenanthrenequinone, similar to other *ortho*-quinones has a very distinctive visible $n-\pi^*$ absorption. Visible absorption band of 9,10-phenanthrenequinone has a small overlap with the absorption of **1**, which allows one to clearly visualize the photochemical release of 9,10-phenanthrenequinone (Figure 1).

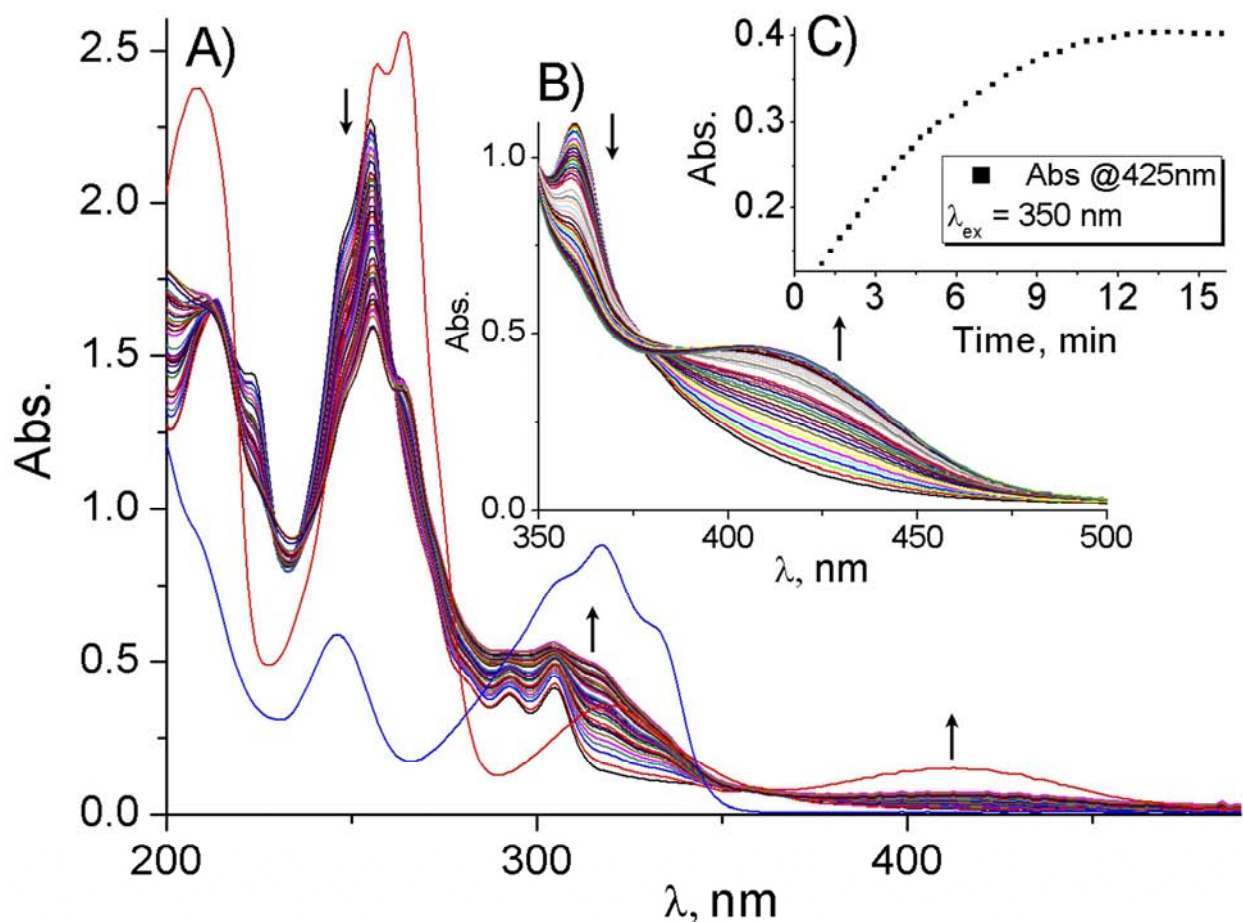


Figure 1. A) Photolysis of 37 μ M acetonitrile solution of **1** upon 350 nm UV light irradiation, (red line – 9,10-phenanthrenequinone, blue line – *N,N*-dimethyl-1,2-di(pyridin-4-ium)ethylene tetrafluoroborate (*N*-methylated alkene); B) Results of the 350 nm light irradiation of a 305 μ M acetonitrile solution of **1**; C) Time evolution of the 425 nm absorption band of 9,10-phenanthrenequinone in 305 μ M solution of **1**.

Upon UV light irradiation of **1**, a pronounced increase of the absorption bands at 320 nm and 425 nm was observed (Figure 1, A). The enhancement of the 425 nm absorption band can be attributed to the release of 9,10-phenanthrenequinone which has a distinctive absorption band at this wavelength (Figure 1, A: red line). The photorelease of 9,10-phenanthrenequinone upon 350 nm UV light irradiation was additionally supported by ^1H NMR experiment (See SI). The increase of the 320 nm absorption band is associated not only with the photochemical release of 9,10-phenanthrenequinone, but also with the formation of the other product of the reverse Schönberg-Mustafa reaction – methylated salt of the substituted alkene, *trans*-*N,N*-dimethyl-1,2-di(pyridin-4-ium)ethylene tetrafluoroborate (Figure 1, A: blue line). A clear decrease of the 255 nm band of **1** is related to the transformation of the initial dihydrodioxin into corresponding photoproducts upon UV light irradiation. Quantum yield of the 9,10-phenanthrenequinone release under UV light irradiation was determined as 1.8 % (for full details, see SI). Time evolution of the 425 nm absorption band of 9,10-phenanthrenequinone (Figure 1, C) shows the progress of the *ortho*-quinone release caused by UV light irradiation.

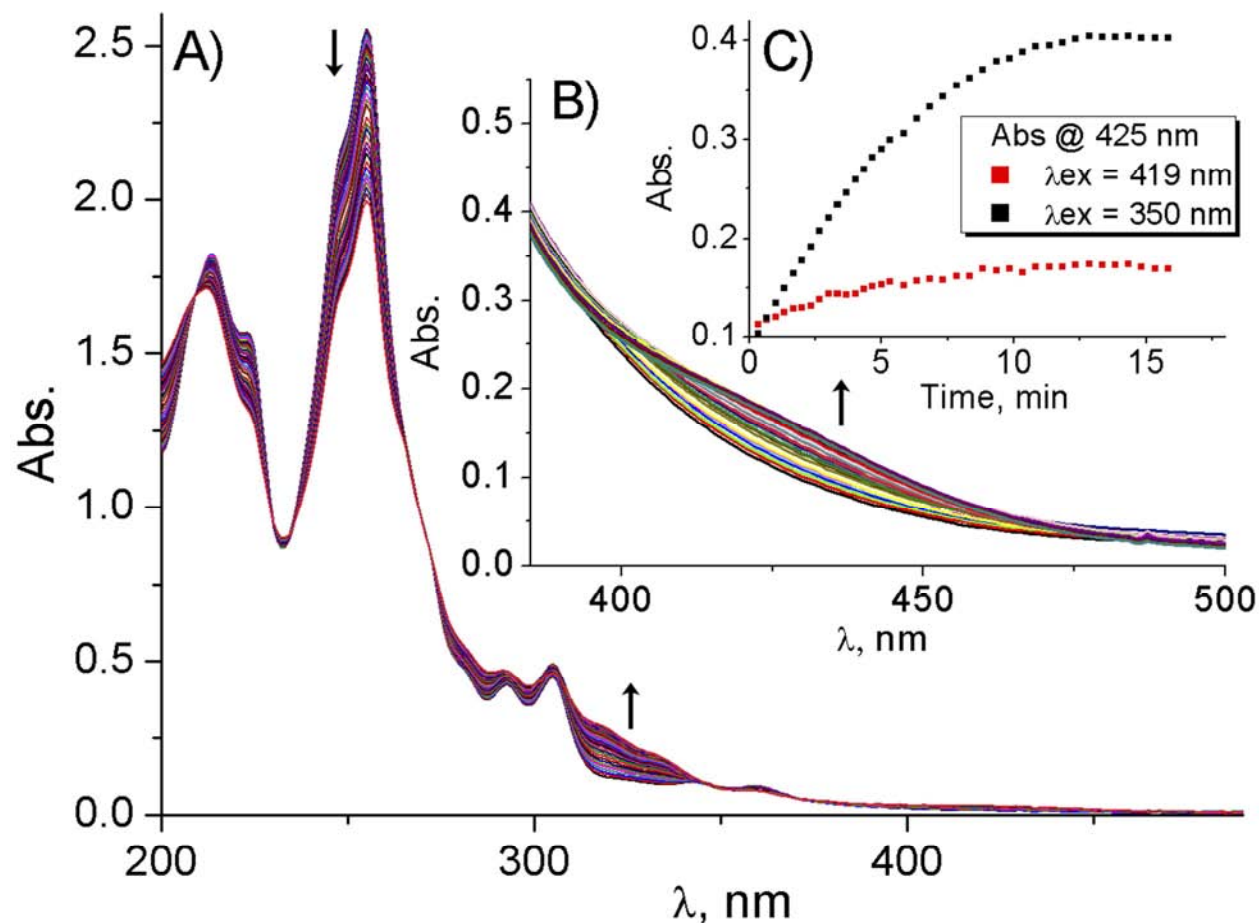


Figure 2. A) Photolysis of 40 μM acetonitrile solution of **1** upon visible light irradiation (419 nm) in acetonitrile; B) 312 μM acetonitrile solution of **1** irradiated by 419 nm light; C) Comparison of the time evolution of the 425 nm absorption band of 9,10-phenanthrenequinone at 419 nm and 350 nm excitation wavelengths.

Visible light irradiation (419 nm) of **1** resulted in the slower 9,10-phenanthrenequinone release (Figure 2, C). This difference can be explained by a higher molar absorptivity of **1** at shorter wavelengths ($\epsilon_{350} = 1960 \text{ cm}^{-1} \text{ M}^{-1}$ compared to $\epsilon_{419} = 550 \text{ cm}^{-1} \text{ M}^{-1}$). Although 9,10-phenanthrenequinone release might take longer time upon visible light irradiation of **1**, the visible light is a less harsh source of stimulus compared to UV light so it could be used in DNA damaging experiments. It was also previously shown that the formation of the quinone radical

anion which triggers DNA damage is an autocatalytic process: the system is activated under visible light irradiation (absorption by the released quinone) and facilitates DNA damage upon continued light irradiation [18a, b].

*3.2 DNA binding mode of **1** studied by viscometry*

Viscometry is considered to be one of the least ambiguous and the most conclusive tests to elucidate the binding mode of a binding agent to DNA [32]. It is well known that classical DNA intercalators induce the DNA base pairs to separate significantly in order to accommodate the binding molecule [33]. This separation causes the DNA helix lengthening upon the addition of intercalative DNA binder. In contrast, the interaction of groove binders with DNA typically results in a bend in the DNA helix that reduces the effect of the groove binders on the DNA helix length which either remains constant or decreases insignificantly upon the addition of the groove binder [34]. Thus, to distinguish the binding mode of **1**, the hydrodynamic method sensitive towards the changes of DNA helix length, i.e. viscometry, was chosen.

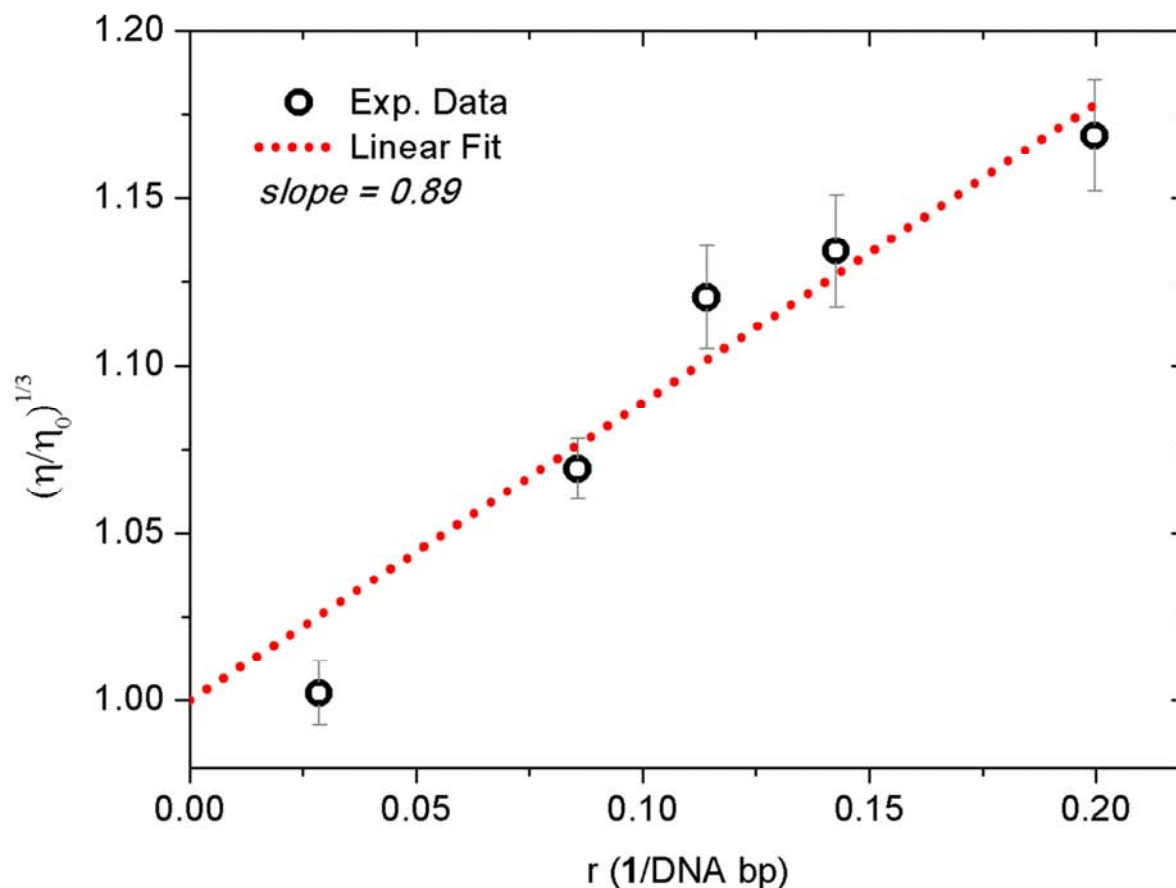


Figure 3. Change of the relative viscosity of a 1 mM CT-DNA solution in 10 mM PB with 100 mM NaCl ($pH = 7.4$) at 24 °C upon the increasing concentration of **1** dissolved in DMSO.

The results of the viscometric titrations of the CT-DNA solution with **1** are shown in Figure 3. It was established that the incremental additions of **1** induce a gradual increase of the relative viscosity of the CT-DNA solution and, thus, the lengthening of the DNA helix. These results allow one to suggest the intercalative mode of binding of **1** to DNA. The linear fit of the plotted data yields a slope of 0.89 when set to intercept the Y-axis at 1 (relative viscosity in the absence of the intercalator). According to Cohen and Eisenberg [35], similar viscometric studies of classical intercalators should give a slope value close to 1 which is in a reasonable agreement with the data obtained for compound **1**.

To further support the intercalative binding mode of **1** and investigate the interactions of this compound with DNA in more details, several spectroscopic techniques were applied to study the changes induced upon DNA binding.

3.3 DNA binding studied by UV-Vis absorption and fluorescence spectroscopy

Interactions of a binder with DNA cause electronic perturbations in the DNA-binder complex. The most common tool applied to evaluate these changes is UV-Vis absorption spectroscopy. A conclusion regarding the intercalative binding mode of compound **1** drawn after the viscosity measurements can be further supported based on the changes in the UV-Vis absorption spectrum of the binder solution upon gradual addition of DNA. For instance, absorption decrease (hypochromic effect) and red shift of absorption (bathochromic shift) have been previously observed for a number of compounds with intercalative mode of binding [36]. Hypochromic effect is thought to originate from π - π stacking interactions between DNA base pairs and the aromatic moiety of an intercalator [37]. The bathochromic shift is related to the coupling between π orbitals of the intercalated part of a molecule and π orbitals of DNA base pairs followed by the decrease in the π - π^* energy gap [38]. Phenanthrene derivatives are known to intercalate between DNA base pairs [39] owing to the aromaticity of phenanthrene. Thus, UV-Vis absorption spectroscopy was chosen to further investigate the interaction of **1** with DNA.

The intercalation process was monitored by observing the changes in the absorption spectrum of **1** upon gradual addition of different double-stranded DNA oligomers: 11-mer, *polyGC*, and *polyAT*. In each case, a hypochromic effect and bathochromic shift were observed and evaluated (Table 1). Values of both hypochromic effects and bathochromic shifts are comparable with the values reported for different DNA intercalating agents [40, 18a]. In addition

to the DNA intercalation, positively charged pyridinium groups of **1** can electrostatically interact with the negatively charged phosphate backbone of DNA [18a].

Table 1. Binding constants, hypochroism and bathochromic shifts of **1** upon its titration with several double-stranded DNA oligomers derived from UV-Vis absorption experiments.

DNA Sequence	K_b (M^{-1}) per DNA sequence	K_b (M^{-1}) per DNA bp	Hypochroism (%)	Bathochromic shift (nm)
<i>polyAT</i>	$(1.9 \pm 0.3) \cdot 10^5$	$(1.7 \pm 0.3) \cdot 10^4$	26	6
<i>polyGC</i>	$(1.5 \pm 0.2) \cdot 10^5$	$(1.4 \pm 0.2) \cdot 10^4$	30	5
11-mer (54 % GC)	$(1.4 \pm 0.1) \cdot 10^5$	$(1.3 \pm 0.1) \cdot 10^4$	24	6

To determine whether **1** exhibits preferential binding to either type of DNA base pairs, we performed two UV-Vis absorption titration experiments with *polyAT* and *polyGC* DNA sequences. The gradual addition of these double-stranded DNA oligomers to a solution of **1** resulted in the decrease of absorption of **1** at 305 nm (by 26 and 30 % for *polyAT* and *polyGC* correspondingly) and red shift of the 305 nm characteristic peak (by 6 and 5 nm for *polyAT* and *polyGC* correspondingly) (Figure 4 and 5). A distinctive isosbestic point at 308 nm in both titrations was observed. The presence of an isosbestic point, a single wavelength at which the absorption coefficients of two species present in the solution are equal [41], is strong evidence of the coexistence of two forms of **1**: unbound to DNA and bound to DNA. Afore described results are an additional indication of the intercalative mode of binding of **1** to DNA [42].

Half-reciprocal plots (Figure 4 and 5, inset C) were obtained based on the data derived from UV-Vis absorption titration experiments of **1** by solutions of *polyAT* and *polyGC* (Figure 4 and 5). Binding constants were calculated according to the equation (1) [29, 30] and gave values of 10^5 order of magnitude when estimated per DNA sequence and of 10^4 when calculated per base pair (Table 1). No significant difference in hypochromic effects and bathochromic shifts was observed upon interaction of **1** with *polyAT* and *polyGC*. However, binding of **1** to *polyAT* appeared to be slightly stronger than to *polyGC* ($K_{polyAT}/K_{polyGC} \sim 1.3$). Majority of intercalators demonstrate preferential binding towards GC rich DNA sequences [43], and fewer intercalators exhibit selective binding to AT-rich DNA sequences. It was previously reported in the literature that phenanthrene derivatives exhibit higher AT binding specificity [44] compared to GC which is in agreement with the results observed in this work. Thus, phenanthrene derivatives might be well suited for the design of photocleavers that target AT sites.

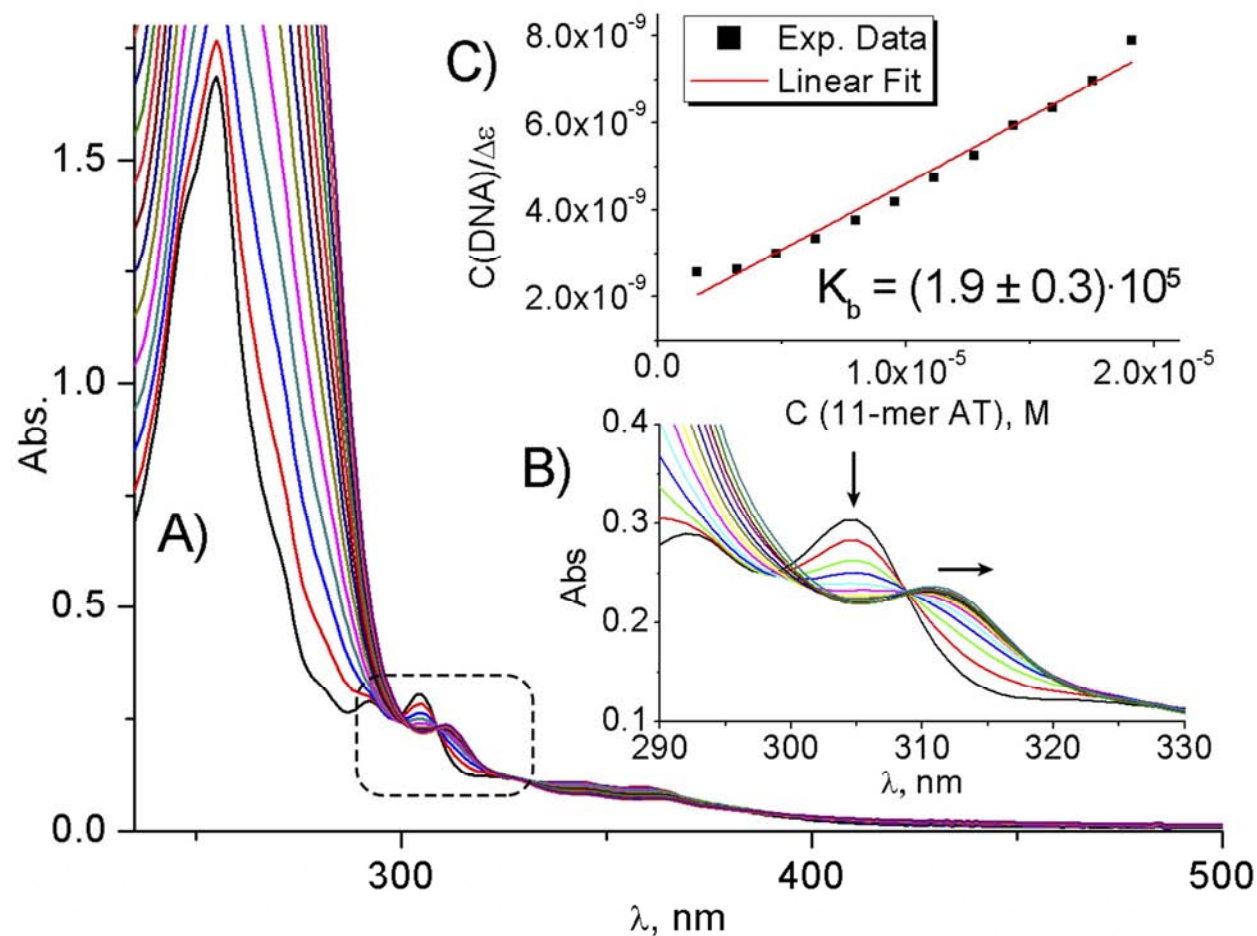


Figure 4. A) UV-Vis absorption titration of **1** (34 μ M) in phosphate buffer by a solution of *polyAT*; B) Enlargement of the 290 nm – 330 nm area to examine the isosbestic point; C) Half-reciprocal plot of **1** binding with *polyAT* DNA determined from the absorption titration data. For full details, see SI.

Changes of the absorption of **1** upon addition of the third kind of DNA oligonucleotide was also monitored by means of UV-Vis absorption spectroscopy (Figure 6). 11-mer DNA sequence containing 54 % of GC base pairs was chosen to compare its binding constant to **1** with the corresponding values for *polyAT* and *polyGC* oligonucleotides and to calculate the binding site size of **1**. Value of the binding constant of **1** to 54% GC 11-mer was close to the binding constant of **1** to *polyGC* and slightly smaller than the one for *polyAT* (Table 1, also see SI). This

data correlates with the assumption on the marginally preferential binding of **1** towards AT-rich DNA sequences.

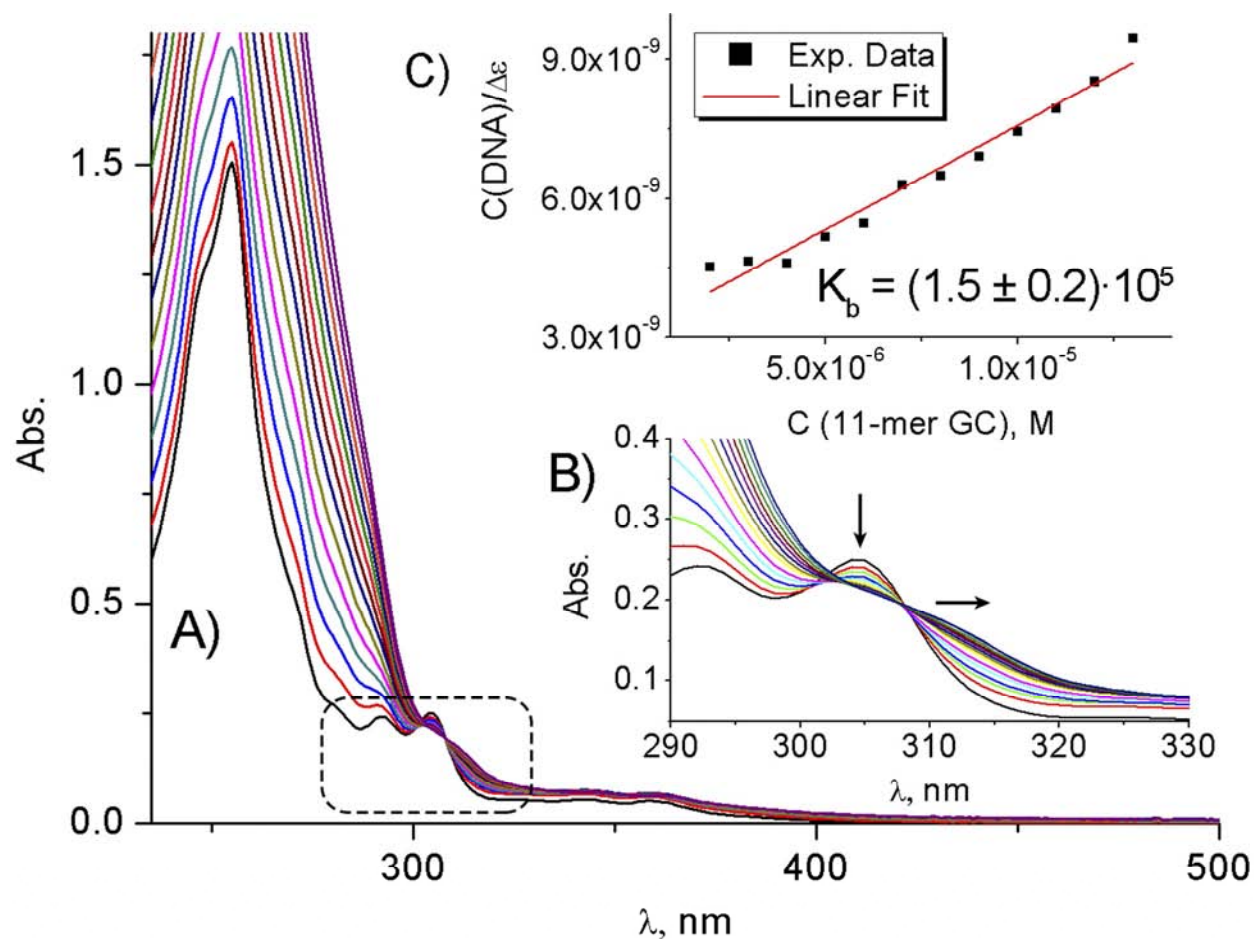


Figure 5. A) UV-Vis absorption titration of **1** (28 μM) in phosphate buffer by a solution of *polyGC*; B) Enlargement of the 290 nm – 330 nm area to examine the isosbestic point; C) Half-reciprocal plot of **1** binding with *polyAT* DNA determined from the absorption titration data. For full details, see SI.

To evaluate the DNA binding site size (n), i.e. the number of DNA base pairs spanned by one molecule of **1**, the absorbance of **1** upon titration with 11-mer DNA sequence was plotted vs the ratio of DNA concentration in base pairs to the concentration of **1** (Figure 6: B). Upon

increasing the concentration of DNA, the 11-mer sequence becomes saturated by the intercalator **1**. After the point of saturation further addition of 11-mer to **1** results in no significant change of the absorbance of **1** at 305 nm. The ratio of 11-mer concentration to the concentration of **1** that corresponds to the saturation point was evaluated by the intersection of two linear plots derived from UV-Vis absorption titration and expressed in the number of base pairs of the DNA sequence spanned by one molecule of **1**. The DNA binding site size of **1** was evaluated as 3.7 ± 0.1 base pairs. The binding site size of **1** is comparable to other intercalators, such as phenanthroline based cobalt complexes ($n \sim 3$ bp) [45], crown ether-annelated styryl dyes ($n = 3.7$ bp) [46] and the derivative of **1** with pyrene aromatic moiety instead of phenanthrene ($n = 4.2$ bp) [18a]. A possible reason for the relatively high value of the binding site size of **1** is the presence of two relatively bulky pyridinium positively charged substituents which extend beyond the phenanthrene plane. This may prevent denser packing of **1** within DNA base pairs stack. Values of binding constants of **1** to different DNA sequences are of the same order of magnitude ($\sim 10^4 - 10^5 \text{ M}^{-1}$) as binding constants of typical intercalators described in literature: pyrene-guanidiniocarbonyl-pyrrole cation [17], hydroxybenzo[b]quinolizinium derivatives [2b] and thio-heterocyclic fused naphthalimides containing aminoalkyl side chains [47]. Based on these data obtained from UV-Vis absorption studies one can conclude that the binding mode of **1** to DNA is intercalative.

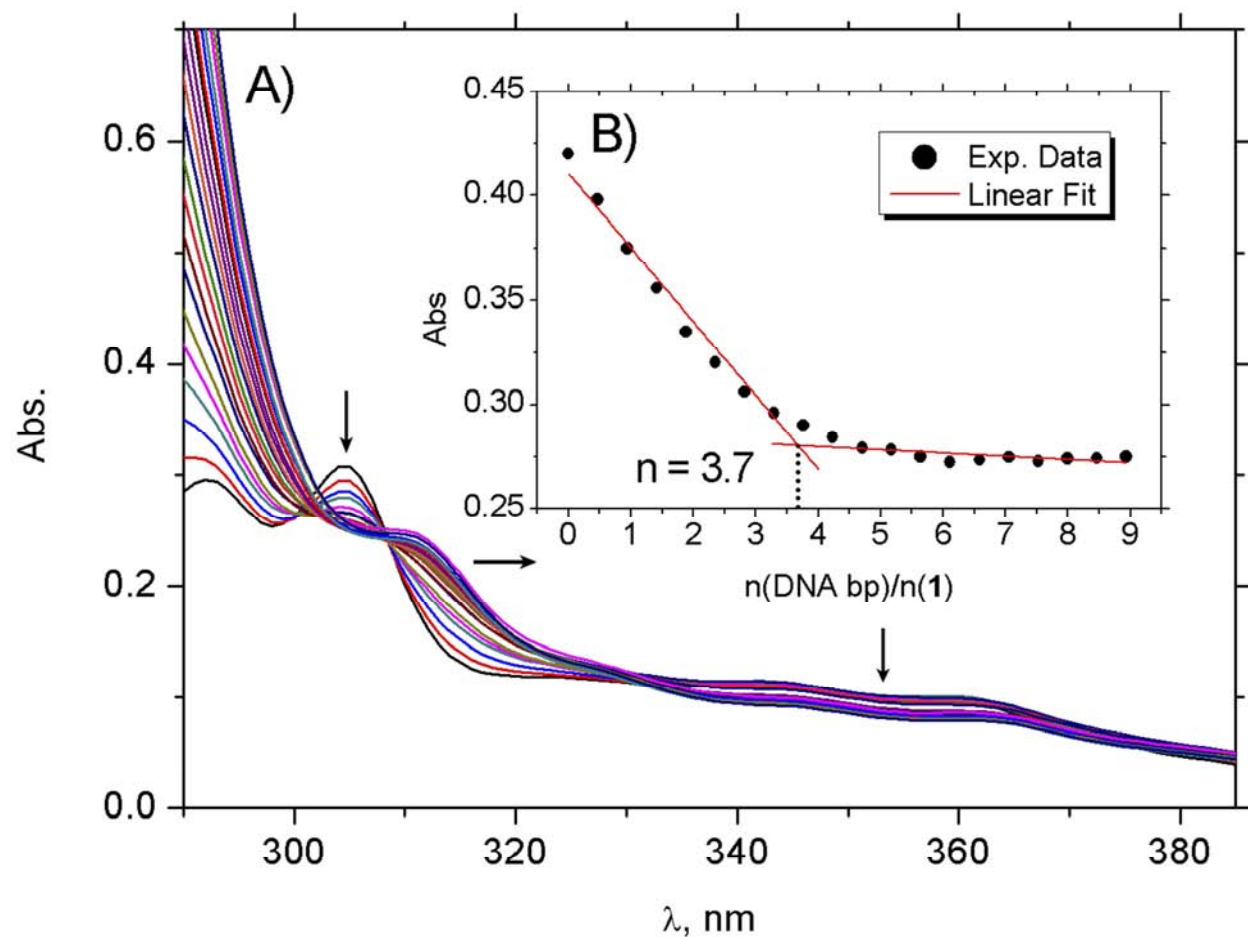


Figure 6. A) Determination of the binding site size of **1**: titration of a 34 μM solution of **1** in phosphate buffer by a solution of 11-mer (final concentration of 11-mer was 30 μM); B) Decrease of the 305 nm absorption plotted vs. the ratio of the 11-mer concentration in base pairs to the concentration of **1**. For full details, see SI.

To support the conclusion of the intercalative nature of the binding mode of **1** to DNA, fluorescence spectroscopy experiment was performed. The emission spectrum of **1** was collected after the excitation at the isosbestic point (308 nm) established previously by UV-Vis absorption titrations of **1** with different double-stranded DNA sequences. This excitation wavelength was chosen to avoid changes in the extinction coefficient of **1** at the excitation wavelength [2b]. Addition of CT-DNA caused the fluorescence quenching of **1** with no significant deviation of the

emission maxima peak at 390 nm (Figure 7). The decrease of the fluorescence intensity is consistent with the formation of **1**-CT-DNA complex through a non-covalent interaction resulting in the insertion of the aromatic planar moiety of **1** between DNA base pairs causing the quenching of the fluorescence signal of **1** [48].

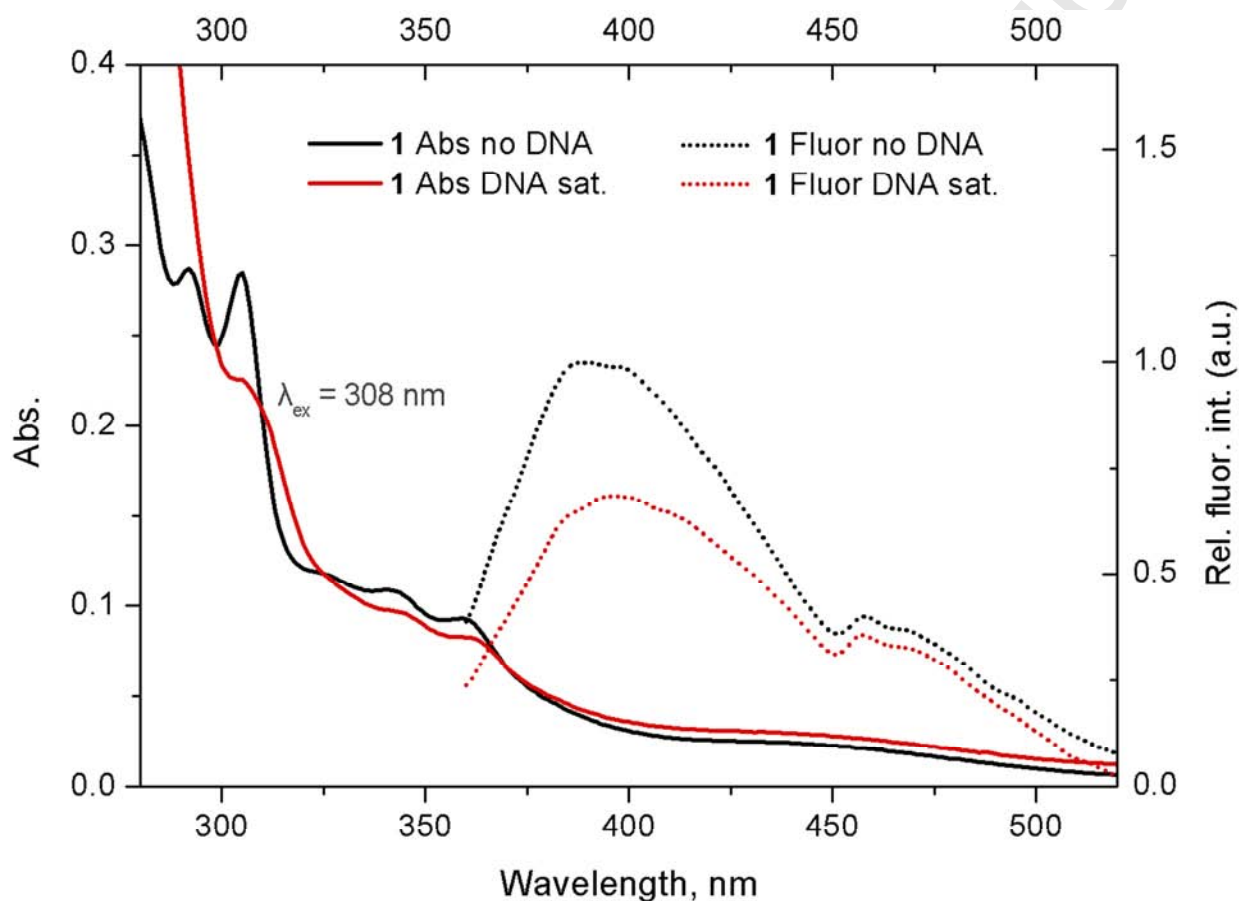


Figure 7. Comparison of the UV-Vis absorption changes (solid lines) with the emission changes of a 33 μM solution of **1** in phosphate buffer (dotted lines) upon addition of CT-DNA. Red curves correspond to the saturation of CT-DNA by **1**.

Distinctive hypochromic effect, bathochromic shift and isosbestic point at 308 nm (Figure 7) observed in the absorption of **1** upon CT-DNA addition along with a pronounced

quenching of the fluorescence of **1** by CT-DNA strongly support our previous conclusion of the intercalative nature of the binding mode of **1** to DNA molecules.

3.4 Conformational changes in DNA upon binding with 1 monitored by Circular Dichroism (CD) spectroscopy

Circular dichroism (CD) spectroscopy is capable of monitoring the absorption difference between right and left circularly polarized light, which makes this technique particularly useful for studies of active chiral compounds, such as DNA [49]. Addition of small molecules that can interact with DNA duplex might trigger DNA conformational changes that can be monitored by CD Spectroscopy [50]. Double-stranded DNA may exist in several different forms, such as A-form, Z-form and B-form. The latter is the most common form of DNA double helical structure. The CD spectrum of this form typically consists of two distinctive bands: a positive band at 260-280 nm and a negative band at 245 nm [51]. The recorded CD spectrum of CT-DNA solution (Figure 8) consisted of a positive band at 275 nm which is attributed to the base pairs stacking and a negative band at 245 nm which arises from helicity of CT-DNA [52]. Positions of these characteristic bands in the CD spectrum of CT-DNA indicated that CT-DNA exists in a B-form. While groove binding of the small molecules to DNA have an insignificant effect on the conformation of DNA and thus no changes in CD spectrum, intercalation of a molecule between DNA base pairs results in the disturbance of the DNA base pair stacking and its helicity that can be observed by distinctive changes in a CD spectrum of DNA [53]. Changes in the CD spectrum of CT-DNA triggered by the interaction with **1** were therefore monitored by means of circular dichroism spectroscopy (Figure 8).

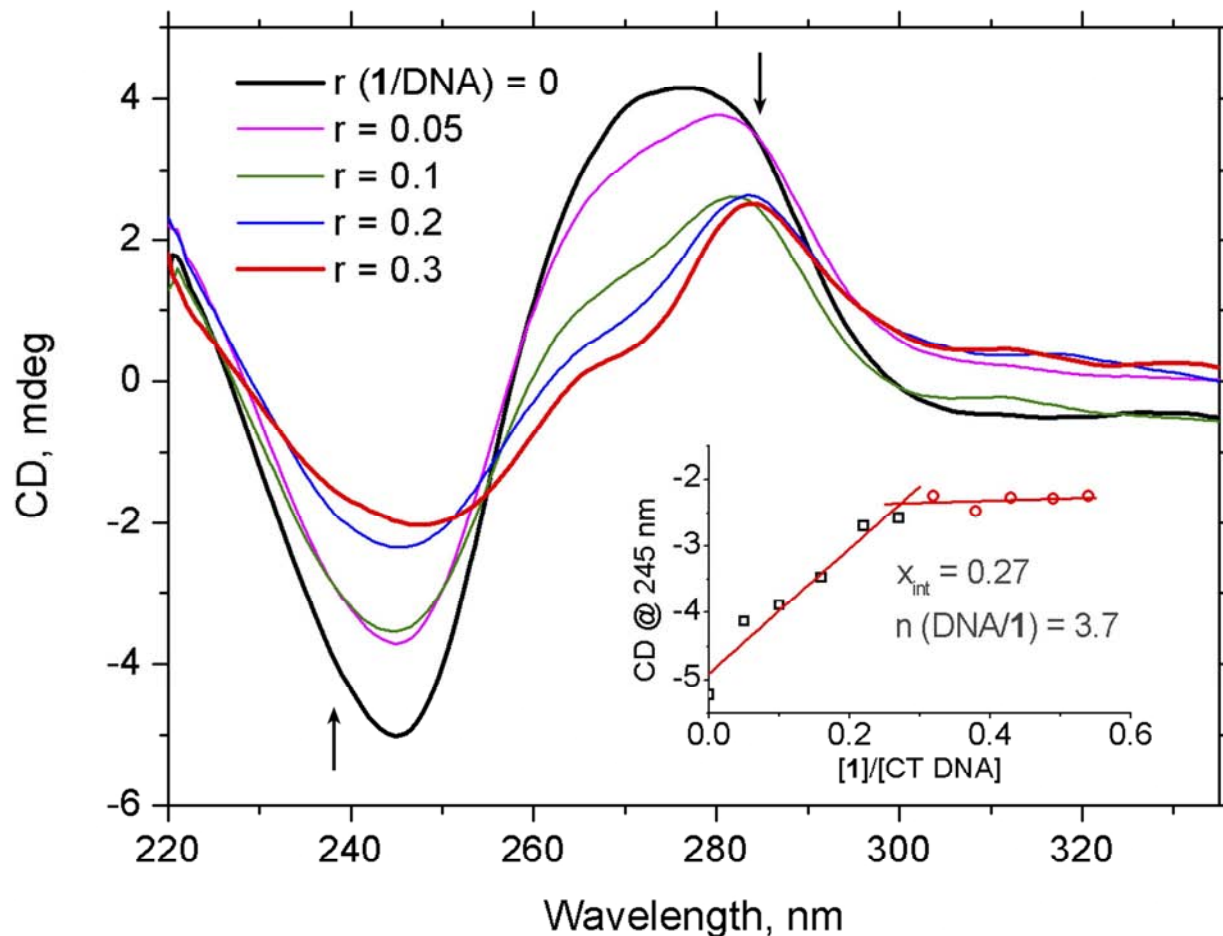


Figure 8. Titration of a 30 μM CT-DNA in phosphate buffer by a solution of **1** monitored by circular dichroism spectroscopy. The molar ratio of **1** to DNA was increased from 0 to 0.5 with 0.05 step (some curves omitted for clarity, for full details, see SI). Arrows show the evolution of CT-DNA CD bands upon the increasing concentration of **1**. Inset – change of the 245 nm CD band intensity plotted vs the **1**/CT-DNA molar ratio.

It is clear from Figure 8 that the gradual addition of **1** to CT-DNA caused major perturbations in the CD spectrum of CT-DNA. The intensity of the pronounced band at 245 nm decreased dramatically by more than 60 % and approached more positive values of ellipticity (Y-axis, expressed in millidegrees or mdeg). After the final addition of **1** to the DNA solution, the 245 nm band was red shifted by 3 nm. The second characteristic CD band of CT-DNA at 275 nm

demonstrated a similar trend. The intensity of the band decreased by > 40 %, and the peak maxima red shifted by ~ 9 nm. However, comparing to the 245 nm absorption, this band decreased towards more negative values of ellipticity during the experiment.

Table 2. Comparison of the characteristic CD bands of B-form of CT-DNA, CT-DNA saturated with **1**, and Z-form of DNA [50, 54].

B-form of CT-DNA	CT-DNA after titration by 1	Z-form
245 nm Negative: -5.0 mdeg	251 nm Less negative: -2.0 mdeg	~ 260 nm Positive
275 nm Positive: 4.1 mdeg	286 nm Less positive: 2.5 mdeg	~ 290 nm Negative

Based on the data derived from the spectroscopic experiment (Table 2), it is reasonable to assume that the incremental addition of **1** triggers a partial CT-DNA conformational transition from B-form to Z-form. Among the distinctive features of DNA Z-form are zig-zag phosphate backbone, left-bended helicity, and characteristic positive CD band at ~ 260 nm and negative band at ~ 290 nm [50, 54]. In general, a CD spectrum of DNA Z-form represents inversed and slightly red shifted version of a CD spectrum of DNA B-form. Interaction of **1** with CT-DNA might induce this inversion as it was previously reported for several other DNA binders [55]. In this particular case, the transition from B-form to Z-form occurred only partially. A partial transition from one DNA form to another could be attributed to the CT-DNA reaching a saturation point at 0.27 ratio of **1**/CT-DNA (3.7 ratio of CT-DNA/**1**, Figure 8, inset). After achieving this ratio, CT-DNA cannot accommodate more molecules of **1**, therefore, no changes are observed in the CD spectrum of CT-DNA upon further addition of the intercalator. Thus,

only a partial transition from B-form to Z-form is observed. The number of DNA base pairs spanned by one molecule of **1** was derived from CD spectroscopic data and calculated as (3.7 ± 0.2) . This result correlates well with the binding site size of 3.7 bp obtained from the UV-Vis absorption binding experiments (Figure 6). After reaching the saturation, the UV-Vis spectrum of **1** showed no red shifts nor absorption decrease (bathochromic shift and hypochromic effect, Table 1) upon further addition of the DNA solution. Thus, the values of the binding site size obtained by means of different spectroscopic methods are in good agreement with each other. Furthermore, a small induced CD peak at ~ 310 nm, a wavelength corresponding to the absorption of **1**, was observed at higher ratios of **1**/CT-DNA. The appearance of a new CD peak at a wavelength corresponding to the absorption of an intercalator is considered to be extra evidence of an intercalating binding mode [2b].

3.5 Optical melting experiments

Interaction of small molecules with DNA might result in a number of different effects, such as conformational changes in DNA structure as discussed in the previous section. The other effect caused by the intercalation of a molecule between DNA base pairs is the stabilization of DNA duplex towards double strand separation. One of the main characteristics of the DNA stabilization is the DNA melting temperature (T_m), which is measured in optical melting experiments. T_m is defined as a temperature at which 50% of DNA double strands are detached into the corresponding single strands. By monitoring this parameter upon addition of small organic molecules one can obtain the information about the nature of DNA binding mode. Hence, strong binding molecules may cause a significant increase in the melting temperature of DNA [56]. DNA duplex itself is stabilized by hydrogen bonds between two strands and base pairs stacking. Intercalators can improve the stabilization of DNA double helix by the insertion

between base pairs resulting in the additional π - π stacking interactions between DNA base pairs and the aromatic moiety of the intercalator. Intercalators typically induce an increase of T_m by 8-12 °C [57].

To evaluate the DNA duplex stabilization by the molecules of **1**, we monitored changes of the 260 nm absorption of the double-stranded DNA 12-mer (5' – GTTAGTATATGG – 3', 33 % GC) upon gradual increase of temperature at different concentrations of the intercalator (Figure 9). The stabilizing effect of **1** was studied for 12-mer/**1** ratios ranging from 0 (T_m of DNA itself) to 21/1, 10.5/1, 5/1 and 3.5/1. Thermal melting curves of DNA-**1** complexes displayed a pronounced shift towards higher values of T_m upon the increasing concentration of the intercalator. The difference between the T_m of the DNA itself and T_m of the DNA complexes with **1** was therefore found to strongly depend on **1**/DNA ratio (Figure 9, inset).

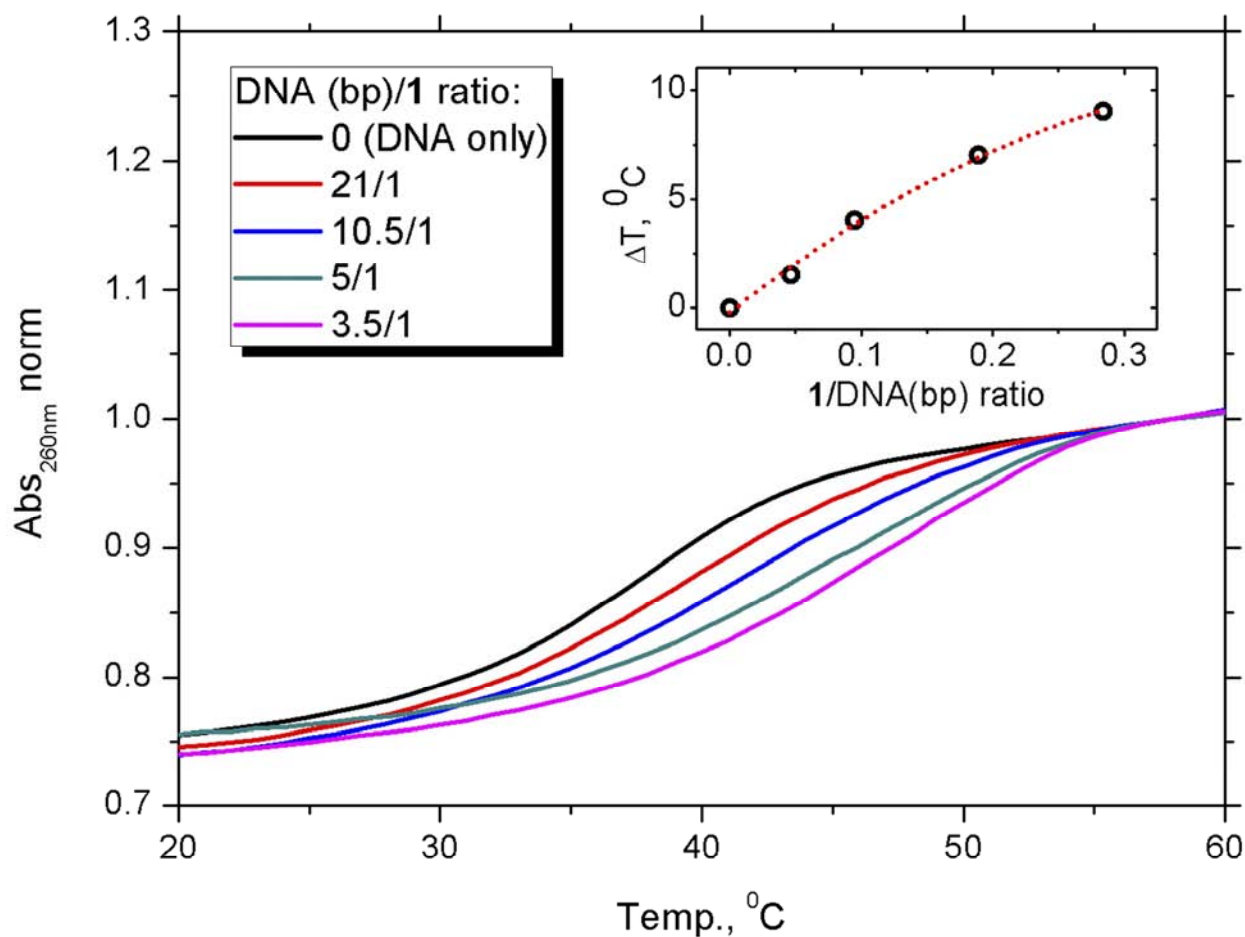


Figure 9. Normalized thermal melting curves of the double-stranded DNA 12-mer solution in phosphate buffer (30.5 μ M in base pairs, black line) and its mixtures with **1** (8.7 μ M final concentration). Inset – ΔT ($\Delta T = T_m(\mathbf{1}\text{-DNA}) - T_m(\text{DNA})$) as a function of the 1/DNA (bp) ratio. For full details, see SI.

T_m of the double-stranded DNA 12-mer itself was calculated as 38 °C from the results of the optical melting experiment which is in agreement with the data reported in the literature for the 12-mer with 33% of GC [58]. Addition of the increasing amounts of **1** to freshly prepared solutions of 12-mer of the same concentration resulted in the sharp increase of the 12-mer T_m , which indicated the stabilizing effect of **1**. The highest T_m of the 12-mer in the presence of **1** (47 °C) was recorded at the 3.5 bp/**1** ratio which is in a good agreement with the results of the UV-

Vis absorption titration and CD Spectroscopy studies (3.7 base pairs per 1 molecule of **1** – the value of binding site size of **1**).

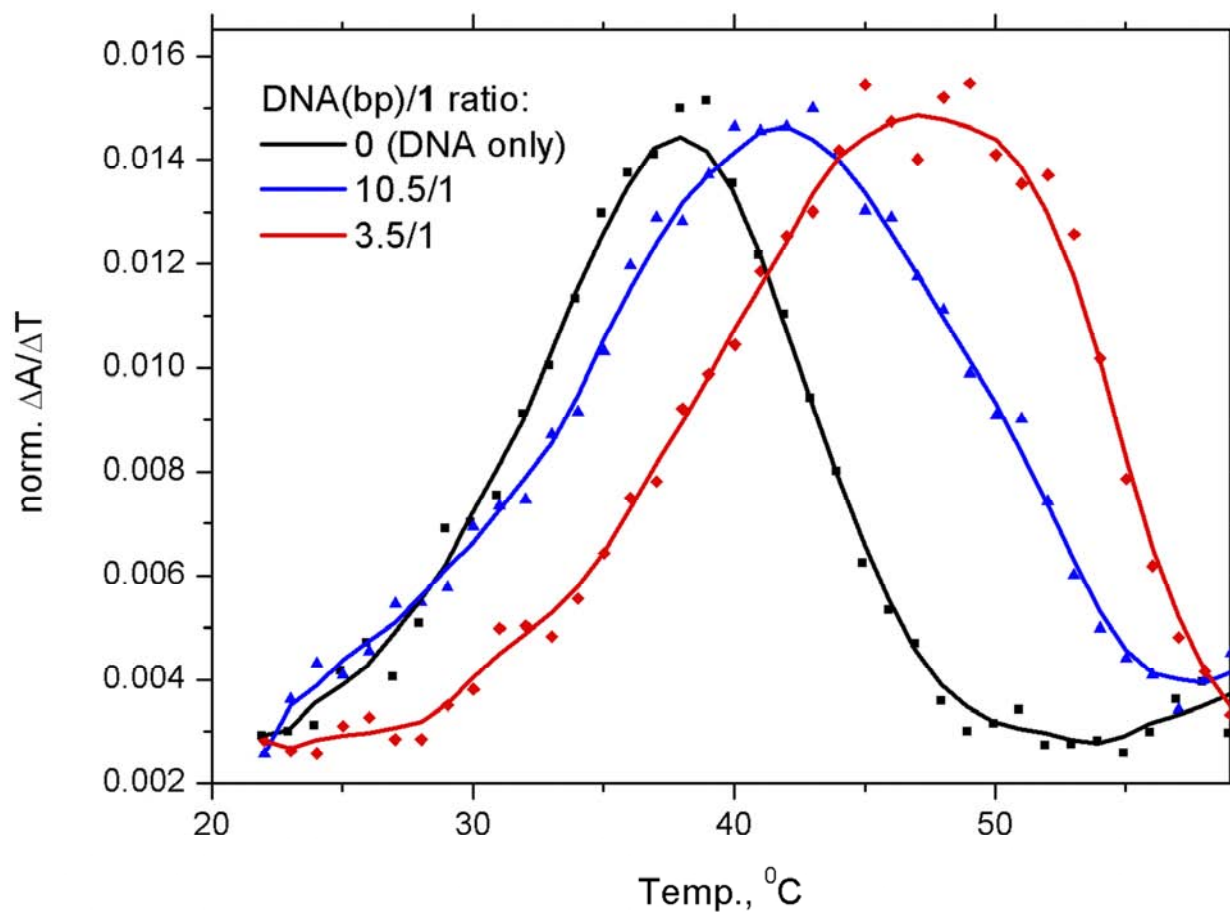


Figure 10. First derivatives of the DNA thermal melting curves; 0 (black line), 10.5/1 (blue line) and 3.5/1 (red line) DNA (bp)/1 ratios. Maxima of the curves correspond to the T_m (some curves omitted for clarity, for full details, see SI).

The results of the DNA optical melting experiments are summarized in Table 3.

Table 3. Summary of the data derived from optical melting studies of the 12-mer in the absence and presence of **1**.

1 / DNA (bp)	DNA (bp)/ 1	T_m , °C	ΔT , °C
0	0	38	0
0.05	20	39.5	1.5
0.09	11.1	42	4
0.19	5.3	45	7
0.28	3.5	47	9

Addition of **1** to a solution of the double-stranded 12-mer induced the stabilizing effect leading to the increase of T_m from 38 °C (12-mer itself) to 47 °C (12-mer saturated with **1**). These results further indicate that **1** binds to DNA duplex in intercalative fashion since the maximum increase of T_m of 12-mer it caused is equal to 9 °C which comparable to ΔT value for reported intercalators [57].

3.5 DNA damaging properties of **1**

The most important goal of any DNA photocleaving agent is to have a potential application as an anticancer drug and, therefore, to damage DNA efficiently [59]. Damage should be preceded by strong binding of the molecule in question to DNA. In previous sections, we showed that **1** intercalates between DNA base pairs evidenced by the viscosity increase of CT-DNA solution upon addition of **1** and further supported by hypochromic effect and bathochromic shift observed during UV-Vis spectroscopic studies of **1** titrated with DNA. The interaction of **1** with DNA caused both DNA structural changes and increased DNA duplex stability. Photolysis of **1** at two different irradiation wavelengths was studied and the

photochemical release of 9,10-phenanthrenequinone was observed. As investigated in previous studies [18a, b], photoinduced unmasking of highly reactive *ortho*-quinones leads to the production of active radical species, which might significantly contribute to light triggered oxidative DNA damage.

To investigate DNA cleaving properties of **1**, Φ X174 photocleavage assay was performed. Φ X174 is a DNA plasmid consisted of 5386 base pairs. It can exist in three different forms: supercoiled (RF I), relaxed or nicked (RF II) and linear (RF III). The nicked form is a result of the single strand DNA cleavage, while the linear form appears only after a double-stranded DNA cleavage. To observe the formation of either nicked or linear forms from supercoiled Φ X174 as evidence of DNA damage, **1** was combined with Φ X174 followed by the irradiation of the mixture and subsequent visualization of the damage by agarose gel electrophoresis. The relative amounts of different Φ X174 forms created after the irradiation were evaluated by densitometric analysis of agarose gel bands.

We used 442 nm (visible) light of He-Cd laser with low output power (70 mW) in order to achieve mild conditions which are important for potential biological applications. UV light was also tested in the DNA damaging experiments. However, our source of irradiation, a 355 nm pulse laser with 1 J/pulse power output, appeared to be too powerful and harsh for Φ X174 plasmid itself. Even small irradiation times (starting from a few laser pulses, 10 ns each) caused the damage in the control sample of Φ X174 plasmid (for full details see SI). Therefore, the less powerful light source and longer irradiation wavelength were chosen for the studies of DNA damaging properties of **1** (Figure 11).

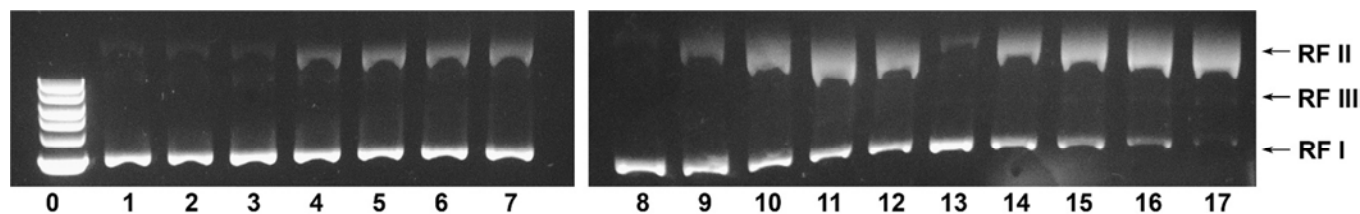


Figure 11. DNA damage caused by **1** at 442 nm irradiation visualized by agarose gel electrophoresis. 0 – 1 kb DNA ladder, 1 – DNA itself stored in the dark, 2 – DNA itself irradiated for 60 minutes, 3-7 – DNA mixed with **1** in 1:50 bp ratio and irradiated for up to 60 min with 15 min intervals (0, 15, 30, 45, 60 min); 8-12 – 1:10 bp ratio, same irradiation conditions, 13-17 – 1:2 ratio, same irradiation conditions. For full details, see SI.

Three series of samples with the same amount of Φ X174 and different concentrations of **1** (1 molecule per 50 base pairs, 10 and 2 base pairs correspondingly) were irradiated by 442 nm light. At low concentration of **1** (1:50 bp, lanes 3-7 on Figure 11) no formation of RF III was observed, while the relative amount of RF II increased from 5 % to 32 % upon the increase of the irradiation time from 0 to 60 minutes. Notably, after 30 minutes of irradiation, the relative amount of the RF II form remained constant (Figure 12, squares).

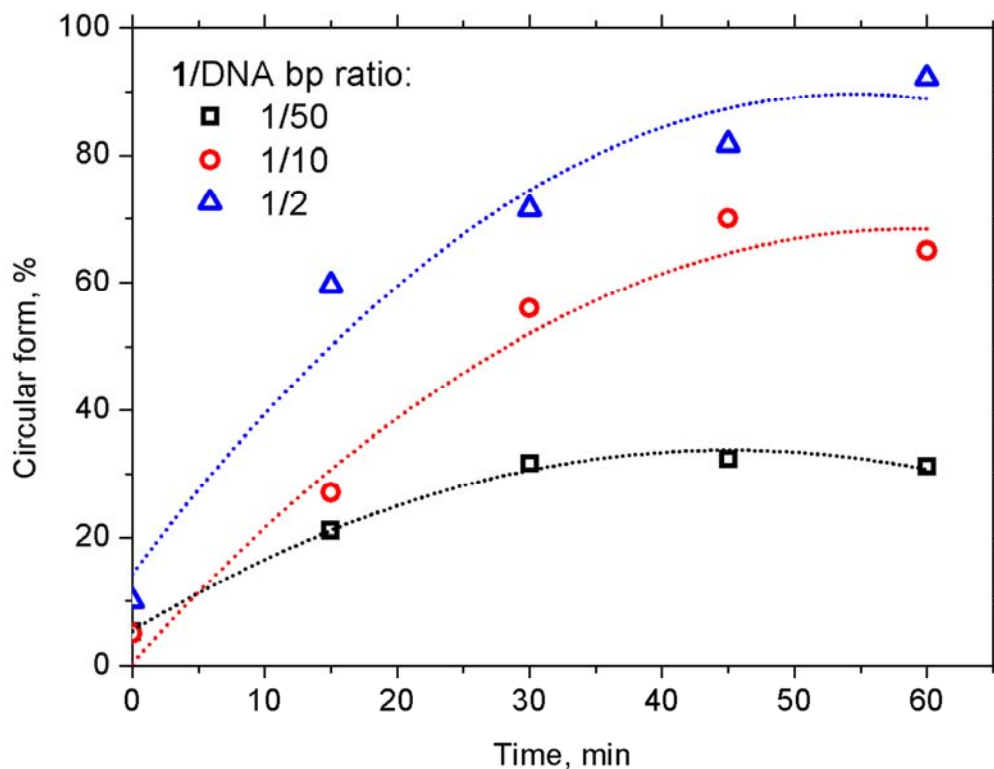


Figure 12. Relative amounts of RF II (the circular form of Φ X174) vs irradiation time. Blue triangles correspond to 1/DNA bp ratio of 1/2, red circles – to 1/10 bp ratio and black squares– to 1/50 bp ratio. Experimental data is fitted with polynomial curves to aid in visualization and to acquire more representative data organization.

According to the binding site size measurements, 1:50 bp concentration is too low to achieve DNA saturation by **1**. Therefore, prolonged exposure to light does not increase the amount of damaged DNA. At 1:10 bp and 1:2 bp concentration of **1** the appearance of bands attributed to the formation of linear RF III is observed (Lanes 8-17 on Figure 11). Densitometric analysis showed the relative amount of RF III did not exceed 5 %. The relative amount of RF II increased from 5% to 70 % and had reached a plateau after 45 min. of irradiation time for 1:10 bp ratio (Figure 12, red circles). This result is well-aligned with the value of the binding site size of **1** calculated from UV-Vis absorption and CD spectroscopy experiments as 3.7 base pairs. The

1:10 base pairs ratio is not high enough to reach saturation. However, it provides a more statistically efficient DNA single-strand damage compared to the one observed for 1:50 bp ratio. At the highest ratio of **1** to DNA base pairs – 1:2 bp, the relative amount of RF II formed after irradiation increased from 10 % to 92 %, and the experimental data had not reached plateau since 1:2 bp ratio of **1** to Φ X174 exceeds the ratio of the binding site size value (1 molec. of **1** per 3.7 bp). Hence, at 1:2 bp concentration of **1** DNA becomes fully saturated by **1**, and 442 nm irradiation of Φ X174 mixed with **1** at this ratio resulted in the most prolific DNA damage compared to other two concentrations of **1** (Table 4).

Table 4. Summarized experimental results of DNA damage caused by different concentrations of **1** (expressed in the ratio of 1 molecule of **1** per X base pairs of DNA) activated by 442 nm light. The relative amount of the relaxed form is derived from the densitometric analysis.

Irradiation time, min	Φ X174 relaxed form, %		
	1:50 bp	1:10 bp	1:2 bp
0	5	5	10
15	21	20	60
30	32	56	72
45	32	70	82
60	31	65	92

The relative amount of the relaxed form of Φ X174 (RF II) showed a steady increase upon increasing the irradiation time in each experimental series. 1:50 bp and 1:10 bp ratios of **1** to DNA base pairs were not high enough to achieve saturation of the DNA, therefore, the relative amount of RF II reached a plateau in both cases. However, 1:2 bp concentration of **1** surpasses

1:3.7 bp ratio (the binding site size value of **1**), and DNA becomes fully saturated by **1**. At 1:2 bp concentration of **1** almost all supercoiled Φ X174 (RF I) was transformed to the relaxed RF II form (92 % RF II).

4. Conclusions

A novel photoactivated DNA cleaving agent **1** was synthesized, characterized and its 9,10-phenanthrenequinone photochemical release was investigated. The interaction of **1** with DNA was studied by means of different analytical methods. Viscometric titration experiment demonstrated

a gradual increase of the relative viscosity of the CT-DNA upon addition of **1**. This result in combination with the UV-Vis absorption titration experiments which showed a significant bathochromic shift and hypochromic effect showed the intercalative fashion of DNA binding. The binding constant of **1** was derived from UV-Vis spectroscopic data and evaluated to be of 10^4 M^{-1} order of magnitude that is comparable to the values of binding constants of typical intercalators. UV-Vis and CD Spectroscopy studies provided data to calculate the binding site size of **1**. Both methods were in a good agreement with each other and indicated a 3.7 base pairs binding site. No significant difference of binding of **1** to either *polyGC* or *polyAT* double-stranded DNA sequences was observed. However, binding constant for *polyAT* appeared to be slightly higher than the one for *polyGC*. The conclusion on the intercalative nature of binding mode of **1** to DNA was supported by fluorescence titration of **1** by CT-DNA. The DNA addition resulted in quenching of the fluorescence of **1** due to the insertion of phenanthrene moiety of **1** between DNA base pairs. Changes in DNA structure and properties associated with interaction with **1** were studied by means of CD spectroscopy and DNA melting temperature analysis. CD spectroscopy experiments showed that addition of **1** to CT-DNA causes a partial conformational

transition from B-form to Z-form of DNA molecule. DNA optical melting experiments demonstrated that **1** contributes greatly to the stabilization of the DNA duplex.

The photocleaving properties of **1** were studied by performing Φ X174 photocleavage assays. Light irradiation of the mixtures of increasing amounts of **1** with supercoiled DNA caused > 90 % supercoiled form relaxation and approximately 5 % of linearization for the higher concentrations of **1** (1:10 bp and 1:2 bp). Results of this study might be used in further development of efficient photoactivated DNA cleavers and DNA intercalators that could bind to specific DNA sequence and in a number of potential biological applications.

Acknowledgements

We thank the R. Marshall and Antonia G. Wilson Chemistry Fund for support of this research. We also thank Dr. Larry Sallans for the mass spectral analysis performed in the Chemistry Department at the University of Cincinnati. We are grateful to Carina B. Haddad and Mariia O. Pushina for the help with quantum yield and fluorescence measurements.

References:

1. (a) Y. H. Du, J. Huang, X. C. Weng, X. Zhou, *Curr. Med. Chem.* 17 (2010) 173;
(b) M. Sunita, B. Anupama, B. Ushaiah, C. Gyana Kumari, *Arabian J. Chem.* 10 (2017) S3367–S3374;
2. (a) G. Ayyannan, P. Veerasamy, M. Mohanraj, G. Raja, A. Manimaran, M. Velusamy, N. Bhuvanesh, R. Nandhakumar, C. Jayabalakrishnan, *Appl. Organometal. Chem.* 31 (2017) 3599;
(b) K. Schäfer, H. Ihmels, E. Porcu, G. Viola, *Chem. Eur. J.* 23 (2017), 370–379;
(c) M. Mariappana, A. Ramasamy, P. A. Prasantha, V. Anbazhaganb, R. Senthilnathanb, A. Jothib, *J. Photochem. Photobiol. A: Chem.* 356 (2018) 617–626.
3. M. J. Waring, *Ann. Rev. Biochem.* 50 (1981) 159-192.
4. (a) A. Soni, P. Khurana, T. Singh, B. Jayaram, *Bioinformatics*, 33(10) (2017) 1488–1496;

- (b) N. Shahabadi, S. Mohammadi, *Bioinorg. Chem. Appl.* (2012), article ID 571913, 8 pages;
5. (a) A. Mukherjee, W. D. Sasikala, *Advances in Protein Chemistry and Structural Biology* 92 (2013) 1-62;
- (b) B. Wang, Z.-Y. Yang, D. Qin, Z.-N. Chen, *J. Photochem. Photobiol. A: Chem.* 194 (2008) 49–58.
6. (a) Laurence H. Hurley, *Nature Reviews Cancer*, 2 (2002) 188–200;
- (b) M.-J. R.P. Queiroz, E. M.S. Castanheira, T. C.T. Lopes, Y. K. Cruz, G. Kirsch, *J. Photochem. Photobiol. A: Chem.* 190 (2007) 45–52.
7. (a) L. S. Lerman, *J. Mol. Biol.* 3 (1961) 18;
- (b) P. J. Bond, R. Langridge, K. W. Jennette, S. J. Lippard, *Proc. Natl. Acad. Sci. U.S.A.* 72 (1975) 5825.
8. (a) S. Li, V. R. Cooper, T. Thonhauser, B. I. Lundqvist, D. C. Langreth, *J. Phys. Chem. B*, 113 (32) (2009) 11166–11172;
- (b) L.B. Hendry, V.B. Mahesh, E.D. Bransome, Jr.D. E. Ewing, *Mutation Research*, 623, Issues 1–2 (2007) 53-71.
9. (a) K. Gurova, *Future Oncol.* 5 (2009) 1685;
- (b) Lv M., Xu H. *Curr. Med. Chem.*, 16 (2009) 4797–4813.
10. B. Armitage, *Chem. Rev.* 98 (1998) 1171–1200.
11. (a) Y. Gao, Z. Ou, G. Yang, L. Liu, M. Jin, X. Wang, B. Zhang, L. Wang, *J. Photochem. Photobiol. A: Chem.* 203 (2009) 105–111;
- (b) N. Chowdhury, S. Dutta, B. Nishitha, S. Dasgupta, N.D. Singh, *Bioorg. Med. Chem. Lett.* 20 (18) (2010) 5414–5417.
12. (a) G. B. Schuster, *Acc. Chem. Res.* 33 (2000) 253–260;
- (b) S. V. Kovalenko, I. V. Alabugin, *Chem. Commun.* (2005) 1444–1446;
- (c) C.G. Fortunaa, U. Mazzucato, G. Musumarra, D. Pannaccib, A. Spalletti, *J. Photochem. Photobiol. A: Chem.* 216 (2010) 66–72.
13. (a) M. S. Safarian, S. Sawoo, C. T. Mapp, D. E. Williams, L. Gude, M.-J. Fernández, A. Lorente, *Chem. Select*, 3 (17) (2018), 4897–4910;
- (b) F. M. Tomlin, C. G. Gordon, Y. Han, T. S. Wu, E. M. Sletten, C. R. Bertozzi, *Bioorg. Med. Chem.*, (2018) Corrected Proof.
14. (a) A. A. Holder, P. Taylor, A. R. Magnusen, E. T. Moffett, K. Meyer, Y. Hong, S. E. Ramsdale, M. Gordon, J. Stubbs, L. A. Seymour, D. Acharya, R. T. Weber, P. F. Smith, G. C. Dismukes, P. Ji, L. Menocal, F. Bai, J. L. Williams, D. M. Crokek, W. L. Jarrett, *Dalton Transactions*, 42 (2013) 11881–11899;

- (b) J. Jiang, D. Liu, Y. Zhao, F. Wu, K. Yang, K. Wang, *Appl Organometal Chem.* 32 (2018) 4468.
15. P. Bhattacharya, A. Basak, A. Campbell, I. V. Alabugin, *Molecular Pharmaceutics*, 15 (3) (2018) 768–797.
16. Pa. S. Nayab, M. Pulaganti, S. K.Chitta, M. Abid, R. Uddin, *J. Fluoresc.*, 25 (2015) 1905–1920.
17. L. Hernandez-Folgado, C. Schmuck, S. Tomic, I. Piantanida, *Bioorg. Med. Chem. Lett.* 18 (2008) 2977–2981.
18. (a) E. F. Khisamutdinov, A. E. Shamaev, K. E. Karabaeva, A. S. Mereshchenko, M. S. Panov, R. Alsulami, P. A. Boda, N. B. Leontis, A.N. Tarnovsky, R. M. Wilson, *J. Photochem. Photobiol. A: Chem.*, 307–308 (2015) 131–146;
- (b) R. N. Alsulami, L. Sallans, E. F. Khisamutdinov, U. Pandey, K. Glusac, R. M. Wilson, *J. Photochem. Photobiol. A: Chem.*, 376 (2019) 224–237.
- (c) E. T. Mack, D. Birzniece, D. R. Veach, W. Coyle, R. M. Wilson, *Bioorg. Med. Chem. Lett.*, 15 (2005) 2173–2176.
19. A. Schönberg, A. Mustafa, *J. Chem. Soc.*, 0 (1947) 997-1000.
20. R.M. Wilson, K. A. Schnapp, A. Harsch, S. Keller, D. J. Schlemm, U.S. Patent 6,018,058, January 25 (2000)
21. K. G. Bendinskas, A. Harsch, R. M. Wilson, R. W. Midden, *Bioconjugate Chem.*, 9 (1998) 555–563.
22. (a) C. E. Rodriguez, Z. Sobol, R.H. Schiestl, *Tox. in Vitro*, 22 (2008) 296–300;
- (b) W. Wang, J. Nykamp, X.-D. Huang, K. Gerhardt, D. G. Dixon, B. M. Greenberg, *Envir. Tox. Chem.*, 28 (8) (2009) 1655–1662;
- (c) Y. Shang, L. Zhang, Y. Jiang, Y. Li, P. Lu, *Chemosphere*, 100 (2014) 42–49.
23. E. T. Mack, A. B. Carle, J. T.-M. Liang, W. Coyle, R. M. Wilson, *J. Am. Chem. Soc.*, 126 (47) (2004) 15324–15325.
24. (a) NR Jena, *J. Biosci.*, 37 (2012) 503–517;
- (b) S. F. AbdulSalam, F.S. Thowfeik, E. J. Merino, *Biochemistry* 55 (38) (2016) 5341–5352.
24. A. A. Farahat, A. Kumar, M. Say, T. Wenzler, R. Brun, A. Paul, W. D. Wilson, D. W. Boykin, *Europ. J. Med. Chem*, 128 (2017) 70e78.
25. (a) G. Felsenfeld, S.Z. Hirschman, *J. Mol. Biol.*, 13 (1965) 407–427;
- (b) H.M. Lee, D.S. Chan, F. Yang, H.Y. Lam, S.C. Yan, C.M. Che, D.L. Ma, C.H. Leung, *Chem. Commun.*, 46 (2010) 4680–4682.
26. J. Marmur, *J. Mol. Biol.* 3 (1961) 208–218.

27. S. Lopez-Gomollon, F.E. Nicolas, *Methods Enzymol.* 529 (2013) 65–83.
28. C. Dedon, *Curr. Protoc. Nucleic Acid Chem.*, 8 (2001) 8.1.
29. D. E. V. Schmechel, D. M. Crothers, *Biopolymers*, 10 (3) (1971) 465–480.
30. A. Wolfe, G. H. Jr. Shimer, T. Meehan, *Biochemistry*, 26 (20) (1987) 6392–6396.
31. A. A. Farahat, A. Kumar, M. Say, T. Wenzler, R. Brun, A. Paul, W. D. Wilson, D. W. Boykin, *Europ. J. Med. Chem*, 128 (2017) 70–78.
32. S. Asaadi, R. Hajian, *J. Mol. Struct.*, 1146 (2017) 861–867.
33. M. Kozsup, E. Farkas, A. Cs. Bényei, J. Kasparkova, H. Crlikova, V. Brabec, P. Buglyó, *J Inorg Biochem.*, 193 (2019) 94–105.
34. M. Sirajuddin, V. McKee, M. Tariq, S. Ali, *Eur. J. Med. Chem.*, 143 (2018) 1903–1918.
35. G. Cohen, H. Eisenberg, *Biopolymers*, 8 (1) (1969) 45–55.
36. (a) L. Wang, M. Tao, G. Zhang, S. Lia, D. Gong, *RSC Adv.*, 5 (2015) 98366–98376;
(b) N. A. Annan, I. S. Butler, H. M. Titi, Y. El-Lazeik, B. J. Jean-Claude, S. I. Mostafa, *Inorganica Chim. Acta*, 487 (2019) 433–447;
(c) M. Nath, Mridula, R. Kumari, *J. Photochem. Photobiol.*, 174 (2017) 182–194;
(d) M. Rodriguez-Cordero, N. Cigüela, L. Llovera, T. González, A. Briceño, V. R. Landaeta, J. Pastrán, *Inorg. Chem. Commun.*, 91 (2018) 124–128;
(e) F. Javed, M. Sirajuddin, S. Ali, N. Khalid, M. N. Tahir, N. A. Shah, Z. Rasheed, M. R. Khan, *Polyhedron*, 104 (2016) 80–90.
37. B. Peng, H. Chao, B. Sun, H. Li, F. Gao, L.N. Ji, *J. Inorg. Biochem.* 101 (2007) 404–411.
38. D. Shiva leela, B. Ushaiah, G. Anupama, M. Sunitha, C. G. Kumari, *J Fluoresc* 25 (2015) 185–197.
39. (a) B. Juskowiak, M. Chudak, *Photochem. Photobiol.*, 79(2) (2004) 137–144;
(b) F. Zhang, Q.-q. Zhang, W.-g. Wang, X.-l. Wang, *J. Photochem. Photobiol. A: Chem.*, 184 (2006) 241–249;
(c) H. Huang, Pingyu Zhang, Y. Chen, K. Qiu, C. Jin, L. Jia, H. Chao, *Dalton Transaction*, 45, (33) (2016) 13135–13145.
40. M. Navarro, E. J. Cisneros-Fajardo, A. Sierralta, M. Fernandez-Mestre, P. Silva, D. Arrieche, E. Marchan, *J. Biol. Inorg. Chem.*, 8 (2003) 401–408.
41. I. A. Vinokurov, J. Kankare, *J. Phys. Chem. B*, 102 (1998) 1136–1140.
42. (a) W.-Y. Li, X.-W. He, J.-G. Xu, *Spectroscop. Lett.*, 33 (5) (2000) 693–704;

- (b) A. Ilangoan, K. Anandhan, K. Mahabir, P. Pakkiri, V. Rajalingam, R. Devanesan, A. Ananth, T. Sivasudha, *Med.Chem. Res.*, 24 (1) (2015) 344–355.
43. (a) J. B. Chaires, *Biopolymers*, 103(9) (2015) 473–479;
(b) S. Sharma, M. Yadav, S. P. Gupta, K. Pandav, S. Kumar, *Chem.-Biol. Interact.*, 260 (2016) 256–262;
(c) J. J. Nogueira, L. González, *Biochem.*, 53 (2014) 2391–2412.
44. W. D. Wilson, Y.-H. Wang, S. Kusuma, S. Chandrasekaran, N. C. Yang, D. W. Boykin, *J. Am. Chem. Soc.* 107 (1985) 4989–4995.
45. K. Nagaraj, G. Velmurugan, S. Sakthinathan, P. Venuvanalingam, S. Arunachalam, *Dalton Trans.*, 43 (2014) 18074.
46. D. V. Berdnikova, O. A. Fedorova, E. V. Tulyakova, H. Li, S. Kölsch, H. Ihmels, *Photochem. Photobiol.*, 91 (2015) 723–731.
47. X. Qian, Y. Li, Yu. Xu, Y. Liu, B. Qua, *Bioorg. Med. Chem. Lett.*, 14 (2004) 2665–2668.
48. (a) C. V. Kumar, E. H. Asuncion, *J. Am. Chem. Soc.* 115 (1993) 8547–8553;
(b) W.-J. Fang, D.-Z. Jin, Y. Luo, H. Li, Y. Zheng, Z. Zhang, H. Gu, S.-S. Zheng, *Bioorg. Med. Chem. Letters* 24 (2014) 3956–3960.
49. R.W. Woody, *Meth. Enzymology* 246 (1995) 34–71.
50. Y.-M. Chang, C. K.-M. Chen, M.-H. Hou, *Int. J. Mol. Sci.* 13 (2012) 3394–3413.
51. D.G. Alexeev, A.A. Lipanov, I. Skuratovskii, *Nature* 1987, 325, 821–823.
52. M.B. Gholivanda, H. Peymanb, Kh. Gholivandc, H. Roshanfekrb, A.A. Taherpourd, R. Yaghoubic, *J. Photochem. Photobiol. A: Chem.*, 338 (2017) 183–19.
53. G. Collins, T.P. Shields, J.K. Barton, *J. Am. Chem. Soc.*, 116 (1994) 9840–9846.
54. V.I. Ivanov, E.E. Minyat, *Nucleic Acids Res.*, 9 (1981) 4783–4798.
55. (a) T. Nishimura, Y. Takeda, N. Shimada, K. Sakurai, *Chem. Lett.*, 36 (3) (2007) 388–389;
(b) E. Sage, M. Leng, *Nucleic Acids Res.*, 9 (5) (1981) 1241–1250;
(c) L. Feng, A. Zhao, J. Ren, X. Qu, *Nucleic Acids Res.*, 41 (2013) 7987–7996;
(d) B. L.Varnado, C. J. Voci, L. M. Meyer, J. K. Coward, *Bioorg. Chem.*, 28 (2000) 395–408.
56. S. Das, G. S. Kumar, *J. Molec, Struct.*, 872 (2008) 56–63.
57. M. F. Hassan, A. Rauf, *Spectrochimica Acta Part A: Mol. Biomol. Spectr.*, 153 (2016) 510–516.

58. R. Owczarzy, Y. You, B. G. Moreira, J. A. Manthey, L. Huang, M. A. Behlke, J. A. Walder, *Biochem.*, 43 (2004) 3537–3554.

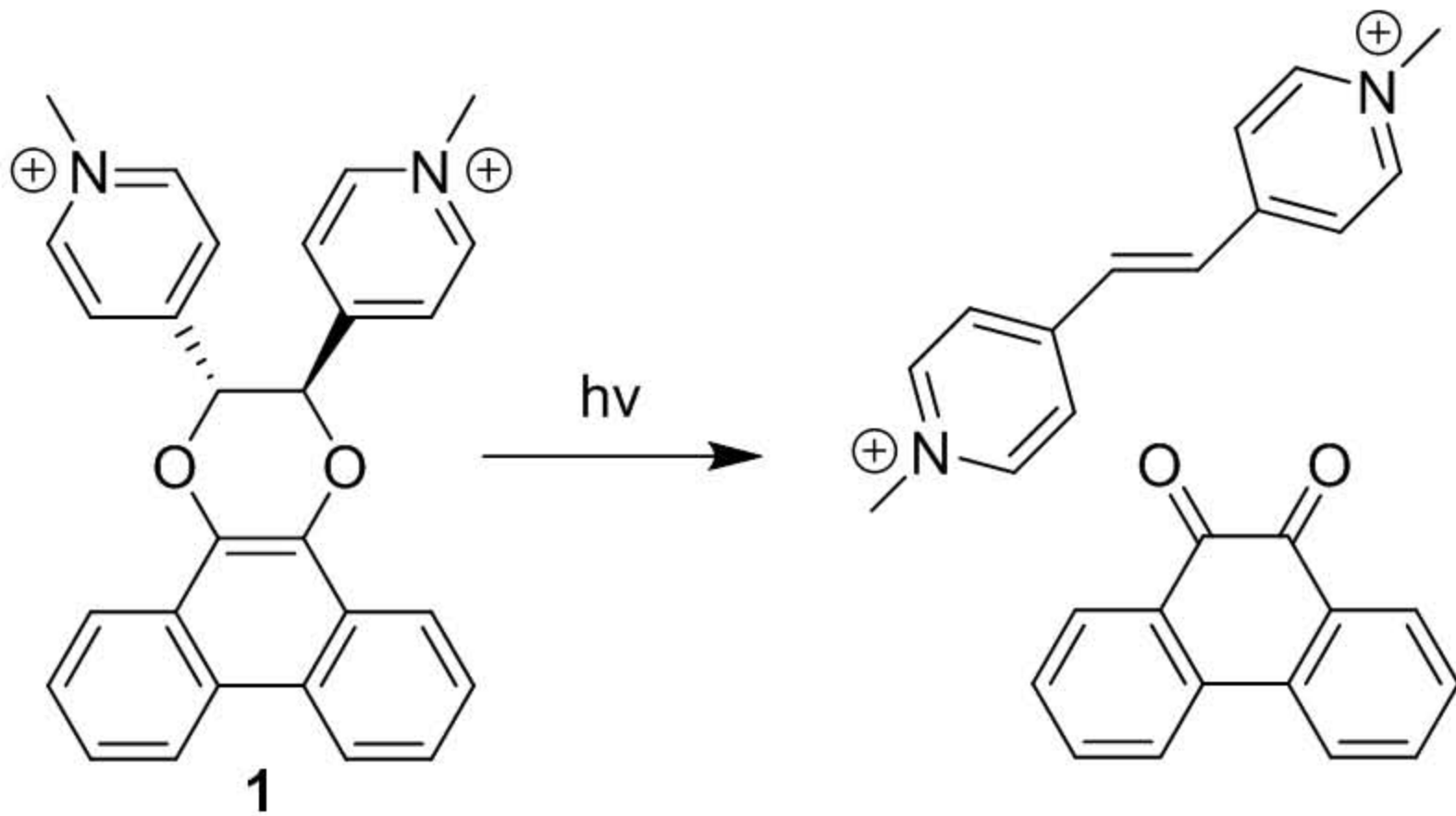
59. P. T. Henderson, B. Armitage, G. B. Schuster, *Biochem.*, 37 (1998) 2991–3000.

Accepted Manuscript

Highlights:

- A novel DNA photocleaving agent, phenanthrene dihydrodioxin (**1**), was synthesized and characterized.
- The photochemical release of 9,10-phenanthrenequinone was studied.
- **1** binds to DNA in intercalative fashion and shows higher affinity to AT rich DNA sequences.
- Interactions of **1** with DNA induce duplex stabilization and transition from B- to Z-form of DNA.
- Phenanthrene dihydrodioxin causes DNA damage upon the light irradiation.

Accepted Manuscript



- Photochemical release of 9,10-phenanthrenequinone
- Intercalative binding mode
- Preferential AT affinity
- Induces B-form to Z-form DNA transition
- Stabilization of DNA duplex
- Photoinduced DNA damage